Planktonic foraminiferal oxygen isotope analysis by ion microprobe technique suggests warm tropical sea surface temperatures during the Early Paleogene

Reinhard Kozdon,[1] D. Clay Kelly,[1] Noriko T. Kita,[1] John H. Fournelle,[1] and John W. Valley[1]

Received 16 September 2010; revised 21 April 2011; accepted 29 April 2011; published 30 July 2011.

[1] Cool tropical sea surface temperatures (SSTs) are reported for warm Paleogene greenhouse climates based on the $\delta^{18}O$ of planktonic foraminiferal tests. These results are difficult to reconcile with models of greenhouse gas–forced climate. It has been suggested that this "cool tropics paradox" arises from postdepositional alteration of foraminiferal calcite, yielding erroneously high $\delta^{18}O$ values. Recrystallization of foraminiferal tests is cryptic and difficult to quantify, and the compilation of robust $\delta^{18}O$ records from moderately altered material remains challenging. Scanning electron microscopy of planktonic foraminiferal chamber-wall cross sections reveals that the basal area of muricae, pustular outgrowths on the chamber walls of species belonging to the genus *Morozovella*, contain no mural pores and may be less susceptible to postdepositional alteration. We analyzed the $\delta^{18}O$ in muricae bases of morozovellids from the central Pacific (Ocean Drilling Program Site 865) by ion microprobe using 10 μm pits with an analytical reproducibility of ±0.34‰ (2 standard deviations). In situ measurements of $\delta^{18}O$ in these domains yield consistently lower values than those published for conventional multispecimen analyses. Assuming that the original $\delta^{18}O$ is largely preserved in the basal areas of muricae, this new $\delta^{18}O$ record indicates Early Paleogene (~49–56 Ma) tropical SSTs in the central Pacific were 4°–8°C higher than inferred from the previously published $\delta^{18}O$ record and that SSTs reached at least ~33°C during the Paleocene-Eocene thermal maximum. This study demonstrates the utility of ion microprobe analysis for generating more reliable paleoclimate records from moderately altered foraminiferal tests preserved in deep-sea sediments.

Citation: Kozdon, R., D. C. Kelly, N. T. Kita, J. H. Fournelle, and J. W. Valley (2011), Planktonic foraminiferal oxygen isotope analysis by ion microprobe technique suggests warm tropical sea surface temperatures during the Early Paleogene, *Paleoceanography*, *26*, PA3206, doi:10.1029/2010PA002056.

1. Introduction

[2] A number of seminal studies helped pave the way for oxygen isotope ratios ($\delta^{18}O$) in biogenic calcite to become what is arguably the single most important geochemical proxy for reconstructing ocean-climate history [*McCrea*, 1950; *Epstein et al.*, 1951; *Urey et al.*, 1951; *Epstein et al.*, 1953; *Emiliani*, 1955, 1966]. This versatile proxy is used to delineate secular variation in a wide range of environmental parameters, and it is the use of $\delta^{18}O$ as a paleothermometer for gauging sea surface temperatures (SSTs) that is the focus of this investigation. Deriving SSTs from planktonic foraminiferal $\delta^{18}O$ records requires consideration of factors such as isotope fractionations related to the physiology of the living foraminifer (i.e., 'vital effects') and the oxygen isotope composition of the ambient seawater [*Duplessy et al.*, 1981; *McConnaughey*, 1989; *Spero and Lea*, 1996; *Rohling and Cooke*, 2003; *Kozdon et al.*, 2009]. Moreover, it is often assumed that planktonic shells (tests) showing no visible signs of dissolution or diagenetic overprinting under the optical microscope are well preserved and that their original $\delta^{18}O$ composition has not changed over time. However, this approach to assessing preservation has been questioned on the grounds that foraminiferal tests can have the superficial appearance of being unaltered as diagenetic calcite can replace primary test structures with little or no change to such delicate structures as wall pores, internal wall layering, or surface ornamentation [*Pearson et al.*, 2001; *Sexton et al.*, 2006; *Pearson et al.*, 2007]. Consequently, failure to recognize and quantify diagenetic alteration is a potential source of

[1]Wisconsin Secondary Ion Mass Spectrometer Laboratory, Department of Geoscience, University of Wisconsin-Madison, Madison, Wisconsin, USA.

0883-8305/11/2010PA002056

error in climate reconstructions based on the δ^{18}O composition of planktonic foraminiferal tests.

[3] Over the last decade, it has come to light that planktonic foraminiferal tests can be differentiated on the basis of their state of preservation [e.g., *Sexton et al.*, 2006]. The tests of living nonencrusted planktonics are translucent and appear *glassy* under the optical microscope. This kind of preservation is generally rare among foraminiferal assemblages preserved in deep-sea sediments. Fossil planktonic tests typically have a *frosty* appearance that likely indicates a modest degree of diagenetic alteration [*Pearson et al.*, 2001], while planktonic tests that have progressed even further through the alteration process have a *chalky* texture.

[4] Planktonic foraminiferal tests are usually more sensitive to diagenetic alteration than the densely constructed tests of their benthic counterparts because they exhibit substantial microscopic porosity and feature large surface areas/mass in order to maintain buoyancy [*Hemleben et al.*, 1989; *Pearson et al.*, 2001; *Sexton et al.*, 2006]. The selection of individual foraminiferal tests for chemical analyses usually involves inspection with a binocular microscope; hence, failure to recognize this insidious form of postdepositional diagenesis, in conjunction with the ubiquity of frosty tests in deep-sea sediments, has led to the general assumption that frosty tests are well preserved. As a result, a great deal of paleoceanographic data have been generated using frosty tests, and the affect of this level of alteration on δ^{18}O warrants further evaluation.

[5] Postdepositional alteration is especially problematic for planktonic δ^{18}O records from tropical regions where surface-to-bottom temperature gradients are most pronounced. For instance, planktonic tests initially grown at warm SSTs (~18–28°C) in modern tropical settings settle to the seafloor where diagenetic calcite, precipitated at much colder bottom water temperatures (~0–3°C), is added to the tests. Hence, secondary, diagenetic calcite can have δ^{18}O values up to 7‰ higher than the original δ^{18}O of the primary, biogenic calcite. Consequently, even minor postdepositional alteration can shift the δ^{18}O of tropical planktonic tests toward higher values, which can be misconstrued as indicating cooler SSTs. Further, the deleterious effects of postdepositional diagenesis may be exacerbated by the fact that tests grown by shallow-dwelling, tropical planktonic foraminifera tend to have thinner walls and/or larger pores than those grown in cooler, high-latitude waters [*Bé*, 1968; *Frerichs et al.*, 1972; *Wu and Berger*, 1989]. Thus, ecophenotypic variation in test thickness/porosity also plays a role in determining the mass balance between the amounts of primary, biogenic calcite and secondary, diagenetic calcite within individual planktonic tests.

[6] However, it is possible that this mode of diagenesis does not uniformly alter planktonic foraminiferal tests because they possess subdomains that lack mural pores that may promote the recrystallization process. Here we demonstrate the possibility to use an ion microprobe to perform in situ δ^{18}O measurements on such subdomains within planktonic tests. The basal areas of "muricae" [*Blow*, 1979], pustular outgrowths at the intersections of interpore ridges along the chamber walls of Early Paleogene mixed-layer dwelling planktonic foraminifera, qualify as optimal targets owing to an absence of mural pores. Thus, the premise for targeting the basal areas of muricae is that these subdomains may be less susceptible to postdepositional alteration than the porous chamber walls and, by extension, may yield more reliable δ^{18}O values (Figure 1). The δ^{18}O of the basal area of muricae can be measured in situ by ion microprobe analysis with 10 μm diameter beam spot and spot-to-spot precision and accuracy of ±0.3‰ (2 SD) [*Valley and Kita*, 2009]. Another advantage that ion microprobe analysis has over conventional analytical techniques involving whole test dissolution is that it conserves much of the original test, so that other types of geochemical analyses may be performed in tandem on the same test. One 10 μm pit removes only ~2 ng of calcite, which is ~10,000 times smaller than the amount of material consumed by automated phosphoric acid devices.

[7] To evaluate the veracity of this technique, we generated a new tropical planktonic δ^{18}O record by ion microprobe for an Early Paleogene section recovered from the central Pacific Ocean (ODP Site 865) that previously yielded cool tropical SSTs [*Bralower et al.*, 1995]. Added motivation for selecting this pelagic section is that it contains a record of the transient global warming event referred to as the Paleocene-Eocene thermal maximum, or PETM [*Bralower et al.*, 1995; *Kelly et al.*, 1996a], which affords the opportunity to assess tropical SSTs during this transient hyperthermal event. Thus, we build upon a published planktonic δ^{18}O record generated using conventional mass spectrometry by constructing a parallel, ion microprobe-generated planktonic δ^{18}O record for this deep-sea archive of the Early Paleogene greenhouse climate state. In doing so, we demonstrate the potential of ion microprobe analysis for extracting the wealth of ocean-climate information encoded within frosty planktonic tests preserved in pelagic sediments.

2. Materials and Methods

2.1. Site Description, Biochronologic Framework, and Core Sampling

[8] The Early Paleogene section selected for study was recovered from a pelagic cap draped atop Allison Guyot in the central Pacific Ocean (18°26′N, 179°33′W), ~2300 km west of Hawaii at Ocean Drilling Program (ODP) Site 865 [*Shipboard Scientific Party*, 1993]. Paleolatitude projections place Site 865 within a few degrees of the equator (2°–5°N) during the Early Paleogene, making it an excellent candidate for evaluating the cool tropics paradox [*Shipboard Scientific Party*, 1993; *Bralower et al.*, 1995]. The section was recovered using advanced hydraulic piston coring, and consists of weakly lithified, homogeneous foraminifer-nannofossil ooze [*Shipboard Scientific Party*, 1993]. Late Paleocene benthic foraminiferal assemblages indicate a midbathyal paleobathymetry (~1300–1500 m), which is comparable to its modern water depth of 1530 m [*Shipboard Scientific Party*, 1993]. The relatively shallow paleodepth ensured that Site 865 remained well above the local calcite compensation depth (CCD) for the entirety of the Early Paleogene [*van Andel*, 1975; *Shipboard Scientific Party*, 1993; *Bralower et al.*, 1995].

[9] A total of 35 samples were taken from ~28 m of a section (77.20–105.00 m below seafloor (mbsf)) recovered within cores from Holes 865B and 865C. For comparative purposes, core samples with previously published SSTs inferred from δ^{18}O and Mg/Ca ratios were specifically

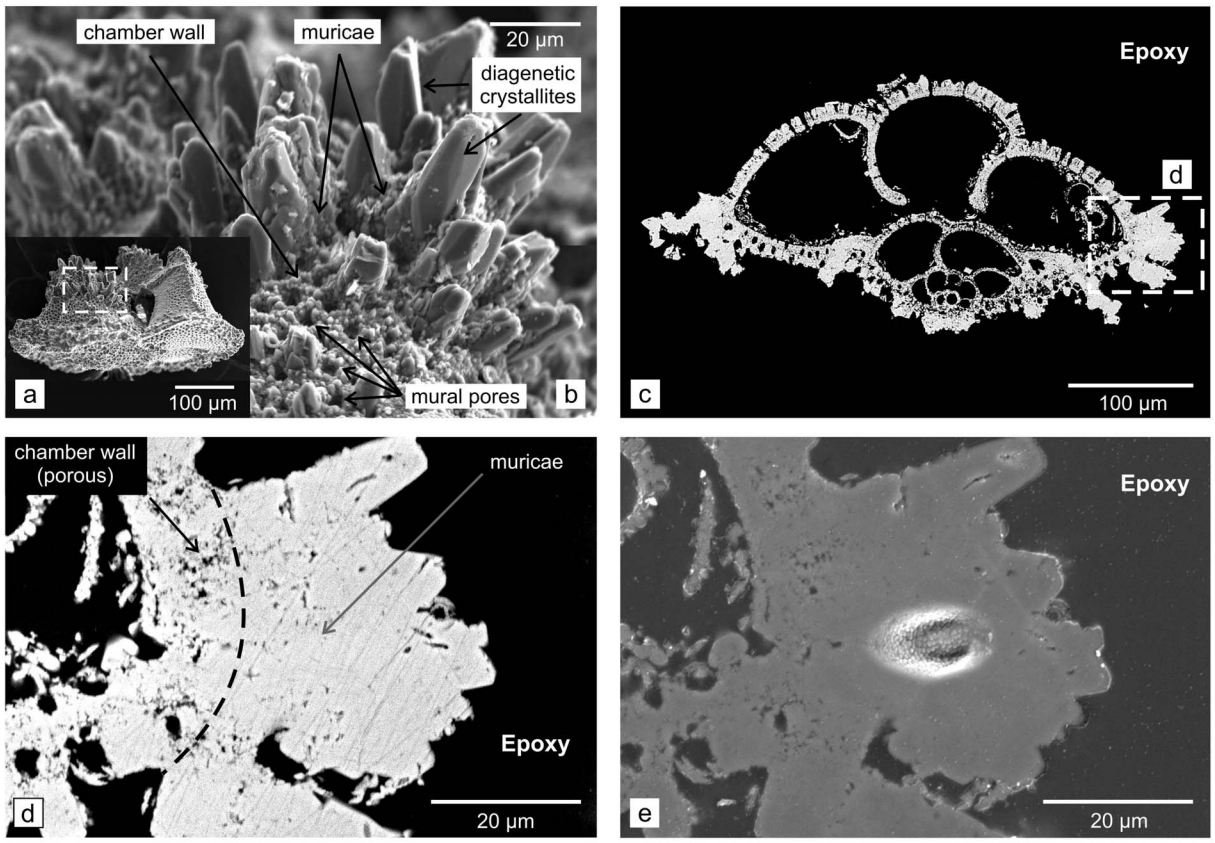

Figure 1. (a) Scanning electron microscope (SEM) image of a test of *Morozovella velascoensis* (ODP Site 865) in edge view. (b) Enlargement of the chamber wall and muricae. Several mural pores are highlighted by arrows. Blade-shaped diagenetic crystallites are cemented on top of the biogenic muricae. (c, d) High contrast SEM backscattered electron images of a polished morozovellid test. Figure 1c is a cross section taken perpendicular to the coiling axis of a *M. velascoensis* test from the 300–355 μm sieve fraction, with a width of 450 μm (Hole 865C, 103.10 mbsf). Figure 1d is an enlargement of a cross section of the same test, showing muricae fused into a keel-like structure at the test periphery. (e) SEM image of the gold-coated sample displaying a ~10 μm ion microprobe pit for δ^{18}O analysis. Textures in the pit are etched by the Cs^+ beam.

selected [*Bralower et al.*, 1995; *Kelly et al.*, 1998; *Tripati et al.*, 2003]. The calcareous nannofossil biozonation constructed for this section indicates that the stratigraphy extends relatively uninterrupted from the late Paleocene through the early Eocene (zones NP9 to NP14a) [*Bralower and Mutterlose*, 1995]. Accordingly, the age model employed in this study was constructed using the published nannofossil biostratigraphy [*Bralower and Mutterlose*, 1995] and the ages assigned to the datums upon which this biozonation is based [*Berggren et al.*, 1995]. Thus, age estimates

Table 1. Sample Core Depths, Assigned Calcareous Nannofossil Zones, and Estimated Ages[a]

Datum[b]	Biozone	Sample ID	Age (Ma)	Sedimentation Rate, Linear (m/Myr)	Depth, 865B (mbsf)	Depth, 865C (mbsf)
FO *D. sublodoensis*	NP14	865B 9H-4 10	49.70	2.67	79.60	
LO *D. orthostylus*	NP13	865B 9H-6 70	50.60	4.00	83.20	
FO *D. lodoensis*	NP12	865B 10H-4 60	52.85	2.84	89.60	
FO *T. contortus*	NP11	865B 10H-5 111/865C 11H-2 134	53.61	2.64/5.6	91.61	91.74
FO *D. diastypus*	NP10	865B 11H-6 70/865C 12H-3 138	55.00	7.62/7.94	102.20	102.68
FO *D. multiradiatus*	NP9	865C 13H-5 80	56.20	9.93		114.60

[a]Core depths [*Bralower and Mutterlose*, 1995] and ages [*Berggren et al.*, 1995] assigned to various nannofossil biostratigraphic datums for calculating linear sedimentation rates that were used to construct a chronostratigraphic framework for the late Paleocene–early Eocene section from Site 865.
[b]FO, first occurrence; LO, last occurrence.

Table 2. In Situ Muricae δ^{18}O Measurements by Ion Microprobe in Morozovellid Species From ODP Site 865 (18°26′N, 179°33′W), Central Pacific, and Muricae δ^{18}O-Inferred SSTs

Hole, Core Section, Interval (cm)	Depth (mbsf)	Age (Ma)	Species	Session/ Analysis Number[a]	Shell/Pit Number	δ^{18}O (‰ PDB)	Avg. δ^{18}O (‰ PDB)	2SE[b]	SST[c] (°C)
865B 9H-2, 70	77.20	48.80	*M. aragonensis*	III-383	26-1	−2.13	−2.93	0.88	26.5
				III-385	27-1	−3.65			
				III-386	27-2	−3.00			
865B 9H-3, 20	78.20	49.18	*M. aragonensis*	III-397	39-1	−2.67	−2.38	0.42	23.8
				III-398	39-2	−2.73			
				III-399	40-1	−2.28			
				III-401	41-1	−1.83			
865B 9H-3, 70	78.70	49.36	*M. aragonensis*	III-395	34-1	−2.58	−2.62	0.08	25.0
				III-396	34-2	−2.66			
865B 9H-4, 10	79.60	49.70	*M. aragonensis*	III-402	46-1	−2.29	−2.86	0.46	26.2
				III-403	46-2	−2.87			
				III-404	47-1	−2.84			
				III-405	47-2	−3.42			
865B 9H-4, 70	80.20	49.85	*M. aragonensis*	III-410	49-1	−3.03	−2.40	0.72	23.9
				III-415	50-1	−2.38			
				III-416	53-1	−1.79			
865B 9H-4, 120	80.70	49.98	*M. aragonensis*	III-427	63-1	−3.04	−3.17	0.28	27.8
				III-428	63-2	−3.71			
				III-429	65-1	−3.05			
				III-431	66-1	−3.18			
				III-432	66-2	−2.89			
865B 9H-5, 70	81.70	50.23	*M. aragonensis*	III-417	57-1	−2.47	−3.14	0.71	27.6
				III-425	60-1	−3.28			
				III-426	60-2	−3.68			
865B 9H-6, 6	82.56	50.44	*M. aragonensis*	III-368	14-1	−3.19	−3.06	0.11	27.2
				III-369	15-1	−3.04			
				III-374	15-2	−3.08			
				III-375	15-3	−2.93			
865B 10H-1, 83	85.33	51.35	*M. aragonensis*	III-434	67-1	−2.63	−3.03	0.45	27.0
				III-440	68-1	−3.41			
				III-441	69-1	−3.04			
865B 10H-2, 60	86.60	51.80	*M. aragonensis*	III-361	7-1	−2.35	−2.29	0.12	27.0
				III-365	12-1	−2.23			
865B 10H-3, 4	87.54	52.13	*M. aragonensis*	III-377	20-1	−2.88	−3.42	0.66	29.0
				III-380	22-1	−3.67			
				III-381	23-1	−3.71			
865B 10H-5, 60	91.10	53.42	*M. subbotinae*	III-442	73-1	−2.99	−3.06	0.35	27.2
				III-444	75-1	−3.34			
				III-445	76-1	−2.81			
				III-446	76-2	−2.43			
				III-447	77-1	−3.10			
				III-448	77-2	−3.67			
865B 11H-1, 20	94.20	53.95	*M. subbotinae*	IV-77	9-1	−3.45	−3.33	0.47	28.6
				IV-97	9-2	−3.65			
				IV-106	11-1	−2.63			
				IV-107	11-2	−3.58			
865B 11H-3, 85	97.85	54.43	*M. subbotinae*	IV-78	11-1	−3.28	−3.38	0.40	28.8
				IV-79	11-2	−3.54			
				IV-99	7-1	−3.82			
				IV-100	7-2	−2.87			
865B 11H-4, 20	98.70	54.54	*M. subbotinae*	III-358	4-1	−3.16	−2.69	0.67	25.4
				III-359	4-2	−2.04			
				III-360	5-1	−2.88			
865C 12H-2, 70	100.50	54.73	*M. velascoensis*	II-121	95-1	−3.56	−3.55	0.57	29.7
				II-122	97-1	−3.95			
				II-127	99-1	−3.14			
865C 12H-3, 0	101.30	54.83	*M. velascoensis*	II-109	78-1	−3.74	−3.84	0.19	31.2
				II-110	79-1	−3.93			
865C 12H-3, 30	101.60	54.86	*M. velascoensis*	II-113	114-1	−3.80	−3.88	0.32	31.4
				II-134	115-1	−4.34			
				II-135	116-1	−3.66			
				II-136	117-1	−3.70			
865C 12H-3, 70	102.00	54.91	*M. velascoensis*	II-98	68-1	−3.52	−3.30	0.45	28.4
				II-100	71-1	−3.07			
865C 12H-3, 110	102.40	54.96	*M. velascoensis*	II-131	110-1	−4.41	−4.28	0.27	33.5
				II-132	110-2	−4.14			
865C 12H-3, 130	102.60	54.99	*M. velascoensis*	II-101	72-1	−3.14	−3.44	0.29	29.1
				II-102	73-2	−3.24			

Table 2. (continued)

Hole, Core Section, Interval (cm)	Depth (mbsf)	Age (Ma)	Species	Session/ Analysis Number[a]	Shell/Pit Number	$\delta^{18}O$ (‰ PDB)	Avg. $\delta^{18}O$ (‰ PDB)	2SE[b]	SST[c] (°C)
				II-103	74-1	−3.69			
				II-104	76-2	−3.69			
865C 12H-3, 146	102.75	55.01	*M. velascoensis*	I-89	1-1	−4.47	−4.26	0.42	33.4
				I-90	1-2	−4.05			
865C 12H-4, 4	102.84	55.02	*M. velascoensis*	II-85	55-1	−3.89	−4.04	0.30	32.2
				II-86	56-1	−4.19			
865C 12H-4, 6	102.87	55.02	*M. velascoensis*	II-66	40-1	−3.26	−3.82	0.70	31.1
				II-70	44-1	−3.73			
				II-97	66-1	−4.47			
865C 12H-4, 6	102.87	55.02	*M. allisonensis*	II-95	62-1	−4.20	−4.24	0.07	33.3
				II-96	63-1	−4.27			
865C 12H-4, 9	102.89	55.02	*M. velascoensis*	II-78	48-1	−3.61	−3.63	0.13	30.1
				II-79	48-2	−3.79			
				II-80	50-1	−3.72			
				II-81	50-2	−3.40			
				II-82	50-3	−3.65			
865C 12H-4, 10	102.90	55.02	*M. velascoensis*	II-47	28-1	−2.97	−3.09	0.13	27.4
				I-86	2-1	−3.11			
				I-88	4-1	−3.20			
865C 12H-4, 10	102.90	55.02	*M. allisonensis*	II-83	52-1	−4.30	−4.12	0.36	32.7
				II-84	52-2	−3.94			
865C 12H-4, 20	103.00	55.03	*M. allisonensis*	II-34	18-1	−3.94	−4.03	0.17	32.2
				II-35	18-2	−4.11			
865C 12H-4, 20	103.00	55.03	*M. velascoensis*	II-38	24-1	−3.59	−3.51	0.17	29.5
				II-39	24-2	−3.42			
865C 12H-4, 30	103.10	55.04	*M. velascoensis*	II-16	9-1	−3.20	−3.39	0.26	28.9
				II-19	10-1	−3.49			
				II-20	10-2	−3.39			
				II-44	26-1	−3.29			
				II-45	26-2	−3.83			
				II-46	27-1	−4.26			
				I-81	1-1	−2.75			
				I-82	2-1	−3.33			
				I-83	2-2	−3.15			
				I-84	3-1	−3.25			
865C 12H-4, 70	103.50	55.08	*M. velascoensis*	II-27	11-1	−4.05	−3.91	0.17	31.6
				II-28	11-2	−3.58			
				II-30	13-1	−4.00			
				II-31	13-2	−3.98			
				II-32	13-3	−3.95			
865C 12H-4, 90	103.70	55.10	*M. velascoensis*	II-140	128-1	−3.95	−3.67	0.57	30.3
				II-141	126-1	−3.38			
865C 12H-4, 120	104.00	55.13	*M. velascoensis*	II-129	101-1	−4.04	−3.88	0.33	31.4
				II-130	101-2	−3.71			
865C 12H-4, 140	104.20	55.15	*M. velascoensis*	II-138	122-1	−3.19	−3.21	0.03	28.4
				II-139	123-1	−3.22			
865C 12H-4, 146	104.28	55.16	*M. velascoensis*	II-61	37-1	−3.91	−3.65	0.53	30.5
				II-63	39-1	−3.38			
865C 12H-5, 0	104.30	55.16	*M. velascoensis*	II-120	94-1	−3.74	−3.74		30.7
865C 12H-5, 70	105.00	55.23	*M. velascoensis*	II-9	3-1	−2.86	−3.37	0.25	28.8
				II-10	3-2	−3.36			
				II-11	4-1	−3.38			
				II-12	4-2	−3.37			
				II-13	6-1	−3.96			
				II-14	6-2	−3.16			
				II-15	6-3	−3.49			

[a]Consecutive analysis number during individual analytical sessions.
[b]Standard error, SE = SD/$n^{0.5}$ of multiple oxygen isotope measurements of muricae within a single core sample.
[c]See section 2.5 for the calculation of SSTs.

for the samples were computed by assuming linear sedimentation rates through the stratigraphic intervals delimited by the first and last occurrences of various nannofossil marker taxa (Table 1).

[10] Twenty samples are from the lower 4.5 m of the study section (100.50–105.00 mbsf), which is entirely within Hole 865C–Core 12H. This basal part of the section spans nannofossil zones NP9 and NP10 making it latest Paleocene to earliest Eocene in age [*Bralower and Mutterlose*, 1995]. Hallmarks such as a negative carbon isotope excursion (CIE) and benthic foraminiferal extinction event constrain the stratigraphic position of the PETM to a narrow interval (~16 cm) within Hole 865C–Core 12H [*Bralower and Mutterlose*, 1995; *Bralower et al.*, 1995].

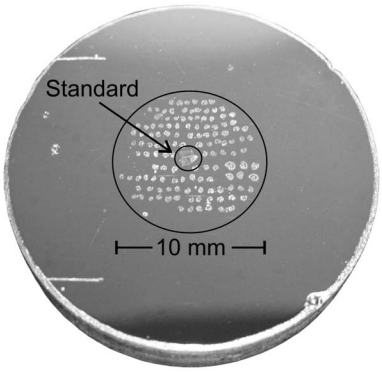

Figure 2. Sample mount for ion microprobe measurements. Approximately 130 morozovellid tests are cast with UWC-3 calcite standard in a 25 mm epoxy mount, ground, polished, and gold-coated.

Moreover, Site 865 is one of only a handful of sites worldwide to preserve a distinctive suite of delicate planktonic foraminiferal morphotypes that occur exclusively during the CIE of the PETM [*Kelly et al.*, 1996a, 1998]. Sample spacing varied through this 4.5 m of section, ranging from an average of ~5 cm within the narrow PETM interval (102.84–103.00 mbsf) to ~30 cm below (103.00–105.00 mbsf) and above (100.50–102.84 mbsf) in Hole 865C–Core 12H (Table 2).

[11] The remaining fifteen samples were taken from the overlying early Eocene section recovered from Hole 865B, Cores 9H–11H. This part of the study section is ~21.5 m thick (77.20–98.70 mbsf) and runs continuously through nannofossil zones NP10–NP14a [*Bralower and Mutterlose*, 1995]. This suite of samples was used to extend the ion microprobe based δ^{18}O record further up-section by generating a long-term, low-resolution record. On average, samples were taken at ~1.5 m increments through this part of the section (Table 2).

2.2. Samples and Preparation

[12] Ion microprobe δ^{18}O analyses were performed on basal domains of muricae in several tropical species (*M. velascoensis, M. allisonensis, M. subbotinae*, and *M. aragonensis*) belonging to the mixed-layer dwelling genus *Morozovella* [*D'Hondt et al.*, 1994; *Norris*, 1996]. For each of the five sample mounts prepared, 80 to 130 morozovellid tests from the 300–355 μm sieve size fraction were handpicked (5 to 7 individual tests for every core sample), cast with 2–3 grains of UWC-3 calcite standard [*Kozdon et al.*, 2009] in the center of a 25 mm round epoxy-mount, ground to the level of best muricae exposure, and polished (Figures 1 and 2). The polishing relief was monitored at submicrometer scale with a Zygo® white light profilometer [*Kita et al.*, 2009]. In order to minimize instrumental bias related to sample position [*Kita et al.*, 2009], each epoxy mount was prepared such that all analytical pits were within 5 mm of the center of the mount. Pit locations for ion microprobe measurements were preselected by backscattered electron imaging (BSE) using a Hitachi S-3400N scanning electron microscope (SEM) in variable pressure mode. At this stage, the sample mounts were uncoated in order to locate nonporous domains within the morozovellid tests with a diameter of at least 10 μm as suitable targets for ion microprobe analyses (Figure 1). Subsequently, the sample mounts were cleaned and gold coated.

2.3. Ion Microprobe Analysis of δ^{18}O in Basal Areas of Muricae

[13] In situ oxygen isotope data were acquired in the WiscSIMS Laboratory at UW-Madison by a CAMECA ims-1280 large radius multicollector ion microprobe [*Kita et al.*, 2009; *Valley and Kita*, 2009] (Figure 3) with analytical conditions similar to those reported by *Orland et al.* [2009]. A $^{133}Cs^+$ primary ion beam with an intensity of ~1.8 nA was focused to a diameter of ~10 μm (sessions 1, 3 and 4) and ~15 μm (session 2). The typical secondary $^{16}O^-$ ion intensity was 3.0×10^9 cps, and $^{18}O^-$ and $^{16}O^-$ ions were simultaneously collected by two Faraday Cup detectors. Charging of the sample surface was compensated by Au coating and an electron flood gun. Grains of UWC-3 calcite standard (δ^{18}O = 12.49‰ [VSMOW]) [*Kozdon et al.*, 2009] were cast in the center of each epoxy mount. Four to five consecutive measurements of UWC-3 calcite standard were performed before and after every set of 9–15 sample analyses. The average precision (reproducibility) for a set of bracketing standard analyses is ±0.34‰ (2 SD). Detailed analytical protocols are described by *Kita et al.* [2009]. A total of 283 measurements were performed, including 95 bracketing standard analyses.

[14] Oxygen isotope ratios of marine carbonates are traditionally expressed relative to PDB. Therefore, final data were converted from calcite δ^{18}O on the VSMOW to the PDB scale by the equation of *Coplen et al.* [1983]:

$$\delta^{18}O[‰\ \text{PDB}] = 0.97002 \times \delta^{18}O[‰\ \text{VSMOW}] - 29.98 \quad (1)$$

After ion microprobe measurements, the appearance and location of analysis pits were imaged by SEM. We consider oxygen isotope data from pits overlapping epoxy resin, cracks, cavities, and inclusions as possibly compromised, and data from these measurements were not used for climate reconstruction. In this respect, it is emphasized that accurate δ^{18}O measurements by ion microprobe cannot be performed on high-porosity domains within the foraminiferal test, limiting suitable areas for in situ δ^{18}O analysis. As seen in Figure 1, a 10 μm diameter analysis pit placed in the morozovellid chamber wall would overlap with large pore spaces, resulting in a drastically reduced secondary ion yield and a nonreproducible shift in the measured δ^{18}O value. This could cause errors that are larger than the natural variation of δ^{18}O within the sample. Thus, δ^{18}O measurements of morozovellid chamber walls were not attempted in this study as the basal portion of muricae provided the only suitable target. Furthermore, δ^{18}O measurements with ion yields less than 90% of that obtained in the nonporous bracketing standard were rejected (all data are reported in Table S1 in the auxiliary material).[1]

2.4. Accuracy of δ^{18}O Analysis by Ion Microprobe

[15] Factors that affect the accuracy of ion microprobe measurements such as sample topography related to sample

[1] Auxiliary materials are available in the HTML. doi:10.1029/2010PA002056.

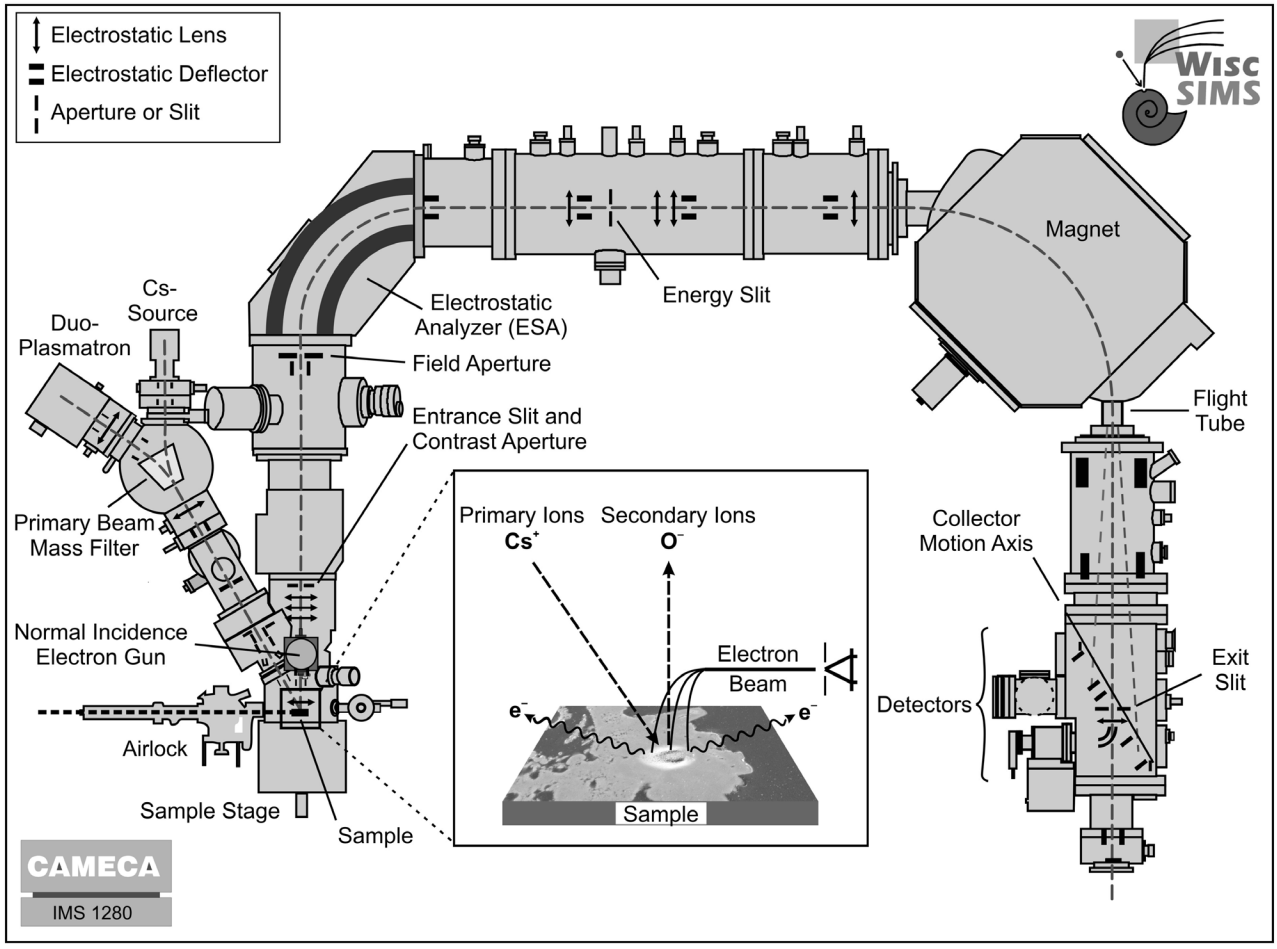

Figure 3. Schematic of the CAMECA ims-1280 ion microprobe, a large radius double focusing mass spectrometer equipped with two primary ion sources (Cs and O). For measurements of oxygen isotope ratio, primary Cs^+ ions accelerated with +10 kV are focused to a spot of 10 μm diameter on the sample surface. Charging of the sample surface is compensated by a normal incidence electron gun. The bombardment of the sample by the Cs^+ beam causes collisions of primary ions with target atoms, sputtering a shallow pit ($\leq$1 μm depth). Ions, neutral atoms, and molecules are ejected from the sample, and secondary ions are accelerated with −10 kV into the mass spectrometer. The secondary ion optics consist of transfer optics from sample to the field aperture, the combination of electrostatic analyzer and sector magnet that sorts ions by mass and focuses in kinetic energy (double focusing), and 10 ion detectors. Transmission of secondary ions through the mass spectrometer is close to 100%. Using a 10 μm beam spot, the secondary ion intensities are sufficiently high so that both $^{16}O^-$ and $^{18}O^-$ are simultaneously analyzed by Faraday Cup detectors.

geometry and polishing relief [*Kita et al.*, 2009], and matrix effects due to sample chemistry [e.g., *Eiler et al.*, 1997; *Valley et al.*, 1998; *Valley and Kita*, 2009] have been thoroughly evaluated in previous studies. To minimize the effect of sample geometry on accuracy, the morozovellid tests were cast with 2–3 grains of UWC-3 standard within 5 mm of the center of the 25 mm epoxy mount (Figure 2). Measurements outside this 10 mm diameter inner circle on the epoxy mount would be less accurate and were not attempted in this study. Further, sample topography was minimized by careful sample polishing and evaluated at submicrometer scale by profilometer [*Kita et al.*, 2009].

[16] Isotope ratios measured by ion microprobe are also subject to systematic instrumental bias caused by differences in sample sputtering, transmission of secondary ions through the mass spectrometer, and by the efficiency of the individual detectors. Therefore, the measured isotope ratios are always biased to the true value, and the UWC-3 calcite standard with a calibrated δ^{18}O of 12.49‰ [VSMOW] [*Kozdon et al.*, 2009] is used for correction. The magnitude of bias varies with the chemistry of the target. For calcite, the instrumental bias of δ^{18}O measurements by ion microprobe changes with the Mg content, and differs by 5.5‰ between analyses of calcite and dolomite for routine analytical conditions at WiscSIMS [*Bowman et al.*, 2009; *Valley and Kita*, 2009]. The UWC-3 calcite standard contains 5450 ppm of Mg [*Kozdon et al.*, 2009], and the Mg content of representative muricae, as determined by electron microprobe analyses, averages 125 ppm (n = 280) for frosty and 137 ppm (n = 112) for glassy foraminiferal tests.

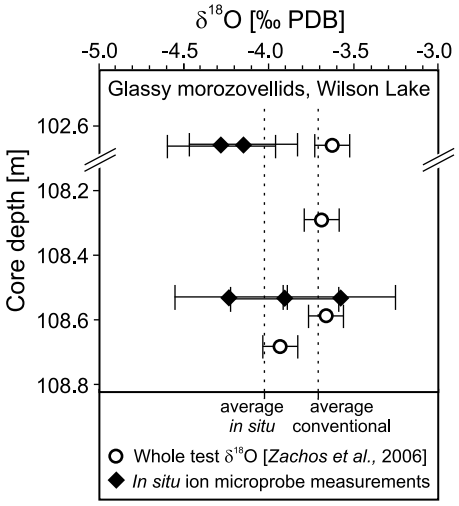

Figure 4. Comparison of published oxygen isotope ratios derived from whole test measurements [*Zachos et al.*, 2006] and in situ ion microprobe analyses of basal areas of muricae made at WiscSIMS. All measurements were performed on glassy morozovellids recovered from the PETM section at Wilson Lake, New Jersey. Error bars connote 2 standard deviations for ion microprobe and conventional whole-test δ^{18}O measurements, respectively. These data indicate that in situ δ^{18}O analyses are indistinguishable from conventional whole test measurements in unaltered planktonic foraminiferal samples, confirming the accuracy of the ion microprobe data. Note that δ^{18}O scale is expanded compared to Figure 5.

Depending on the Mg content at the spot location on the muricae, the cumulative difference in instrumental bias for δ^{18}O between the UWC-3 calcite standard and the foraminiferal test is <0.2‰ and therefore within analytical error. Consequently, the matrix effect correction was not adjusted for different X_{Mg}.

[17] The UWC-3 calcite standard has a δ^{18}O of 12.49‰ [VSMOW] that is significantly lower than the average δ^{18}O of calcite at the base of muricae [~27.5‰ VSMOW or −3.3‰ PDB]. Isotope analyses by ion microprobe (secondary ion mass spectrometry) have been shown to be linear with no differences in bias due to changes in oxygen isotope ratio. Nevertheless, the impact of such a large 15‰ difference between sample and standard is evaluated. *Ferry et al.* [2010] analyzed UWC-1, a second calcite standard with a δ^{18}O of 23.36‰ (VSMOW) [*Bowman et al.*, 2009], in addition to UWC-3 calcite in a single session. The instrumental bias determined for UWC-1 and UWC-3 is within analytical error identical. Furthermore, the linearity and gain of the Faraday Cup amplifiers are monitored using the built-in calibration routine.

[18] In order to further verify the accuracy of in situ analysis of biogenic foraminiferal calcite by ion microprobe, the δ^{18}O of basal areas of muricae in unaltered, glassy morozovellid tests from the PETM section at Wilson Lake (New Jersey) were analyzed and compared to published whole test δ^{18}O values [*Zachos et al.*, 2006]. Although the δ^{18}O data sets are sparse owing to the limited amount of suitable material available, this comparative approach indicates that the ion microprobe measurements are in general agreement with the published whole test values (Figure 4). The δ^{18}O values of basal areas of muricae are statistically indistinguishable from the published whole-test δ^{18}O values as the two data sets are within analytical error of one another over the lower part of this PETM record, while a slight offset (~0.6‰) exists between the two data sets in the uppermost sample. The minor offset seen in the uppermost sample, however, most likely reflects the natural range of δ^{18}O variation among individual morozovellid tests from the same population, which is typically on the order of ~1.0‰ [*Thomas et al.*, 2002]. In addition, previous studies have reported similar agreement between in situ measurements of oxygen isotope ratios in planktonic foraminiferal tests and data from conventional phosphoric acid extraction and gas-source mass spectrometry. *Kozdon et al.* [2009] assessed the intratest δ^{18}O variability in the modern planktonic foraminiferal species *N. pachyderma* (sinistral) from North Atlantic core tops, and found that the in situ measurements of the gametogenetic calcite are within analytical error of published δ^{18}O values of pooled specimens from the same core sample [*Simstich et al.*, 2003].

2.5. Calculated SSTs Based on in Situ δ^{18}O Measurements

[19] Calcification temperatures based on δ^{18}O analysis by ion microprobe were calculated using the fractionation factor for calcite and water determined by *Kim and O'Neil* [1997]:

$$1000\ \ln\alpha\ (\text{calcite} - H_2O) = 18.03\left(10^3 T^{-1}\right) - 32.42\ \ (T \text{ in K}) \tag{2}$$

The results from these inorganic precipitation experiments match the temperature versus δ^{18}O relationship derived from cultured tropical planktonic foraminiferal tests [*Erez and Luz*, 1983; *Bemis et al.*, 1998].

[20] Similar to previous studies that used conventional analytical approaches, no adjustments for secular trends in seawater δ^{18}O or regional variations in the oxygen isotope ratio of seawater were applied. These factors are small, but poorly constrained [cf. *Pearson et al.*, 2007], and seawater δ^{18}O is assumed to be −0.5‰ [SMOW] [*Zachos et al.*, 2006]. Thus, assumptions are comparable to previous studies and the relative differences in temperatures are not affected.

2.6. Mg/Ca Measurements by Electron Microprobe

[21] The chemical composition of morozovellid muricae was analyzed using the Cameca SX51 electron microprobe at UW-Madison Department of Geoscience. Fully quantitative analyses (mineral standards, background subtracted, and matrix corrected) were performed using Probe for EPMA software. In order to generate Mg/Ca maps, EPMA measurements in muricae were performed with a point-to-point spacing of 3 μm on carbon-coated samples.

[22] Whereas in other situations a defocused beam would be utilized due to the beam-sensitive nature of calcite, here the small size of the target required a tight beam. An accelerating voltage of 15 kV with 10 nA Faraday current and a tightly focused beam were used, with a counting time of 10 s on the peak and 5 s on each of two background

positions. These analyses were performed using the "Time Dependent Intensity" (TDI) feature of the Probe for EPMA software, where Ca and Mg were measured in 2 s pulses and counts were plotted against time, with extrapolation to time = 0 s as the true count rate. It is notable that Ca counts increased ~7% for the duration of this procedure, whereas Mg counts did not define any noticeable trend. This correction has a small effect on quantitative analyses, but does not affect the relative differences seen for X-ray maps of Mg/Ca ratio.

[23] The natural carbonate standards Delight Dolomite and Callender Calcite were used for Mg and Ca, respectively. Mg-Kα X-rays were measured on two spectrometers and aggregated. Carbon was calculated within the matrix correction, being allocated as one atom of carbon to 3 atoms of oxygen, and oxygen by stoichiometry to the cations measured, thus analytical totals of 98–100.5 wt.% are a measure of accuracy. For the analyses of the glassy foraminiferal test, Al, Si, Fe and Mn were added to the measurement (detection levels of these elements 0.03, 0.03, 0.07 and 0.07 wt.% respectively). In contrast to the frosty foraminiferal test, TDI treatment for Ca showed no increase or decrease in count rate with time.

[24] Recent Monte Carlo modeling of electron-solid interaction demonstrates a little appreciated fact in EPMA: the size effect. This stems from the fact that some portion of the generated X-rays are produced outside the primary electron excitation volume, and come from secondary fluorescence (by primary X-rays produced by beam electrons) of the region up to tens of microns (in WDS) and hundreds of microns (in EDS; the solid angle is >10 times larger than in WDS) away from the beam impact point. This becomes a significant problem for two cases: trace element analysis (where the element of interest may be present in much higher concentration outside the primary excitation volume), and where the standard and unknown are significantly different in size. *Fournelle* [2006] reported that analytical totals of modeled small grains are lowered by several percent when the standard is several orders of magnitude larger. Some analyses in the glassy foraminiferal test that were placed within a few μm from the outer chamber wall obtained totals of 96% or less; which is consistent with the size effect. These measurements are not included in the Mg/Ca ratio maps and are shown as white areas.

3. Results

3.1. Variance in the $\delta^{18}O$ Data of Individual Tests and Single Samples

[25] Two or more in situ $\delta^{18}O$ measurements were performed in muricae bases of 32 individual morozovellid tests whereas the other specimens were analyzed once (Table 2). On average, multiple $\delta^{18}O$ measurements within the same test vary by 0.33‰ (66 analyses in 31 specimens, one sample excluded), which is about the same as the average spot-to-spot precision of ±0.34‰ (2 SD) achieved in the standard grain. The only notable exception is found in one test of *M. subbotinae*; two measurements of $\delta^{18}O$ within the same specimen vary by 1.1‰.

[26] In situ $\delta^{18}O$ measurements from multiple morozovellid tests in a single sample typically vary by 1‰–1.5‰ (Table 2 and Figure 5). This degree of intraspecific variability in $\delta^{18}O$ is not surprising given that such factors as the species' seasonal distribution and habitat depth range are known to contribute to such variation in living planktonic populations [e.g., *Thomas et al.*, 2002; *Waelbroeck et al.*, 2005]. Moreover, the time averaging effects of sediment mixing processes (bioturbation) are known to be another source of intraspecific stable isotopic variation [*Kelly et al.*, 1998]. That said, a comparable intraspecific $\delta^{18}O$ variability of ~1.2‰–1.5‰ is reported from conventional acid dissolution measurements of individual tests belonging to the modern tropical planktonic species *Orbulina universa*, *Globigerinoides sacculifer*, and *Globigerinoides ruber* picked from a single core sample [*Waelbroeck et al.*, 2005]. Thus, measurements of $\delta^{18}O$ in basal areas of muricae do not induce a larger variance in $\delta^{18}O$ than conventional analytical approaches of whole specimens. In order to minimize the effect of natural variability, the standard error of the mean can be improved by increasing the sample size or by averaging the results from replicate analysis [*Schiffelbein and Hills*, 1984; *Schiffelbein*, 1986].

3.2. Secular Variation in the $\delta^{18}O$ Record

[27] In situ analyses of $\delta^{18}O$ in muricae bases of morozovellid tests from Site 865 spanning the first ~5 Ma of the early Eocene are centered on −3‰ (PDB, $n = 61$) and are on average 1.3‰ lower than published conventional "whole-test" data from age-equivalent core samples that average −1.7‰ [*Bralower et al.*, 1995] (Figure 5a, open circles). However, there are rare instances where muricae-$\delta^{18}O$ values of early Eocene specimens temporarily converge upon published whole test values (Figure 5a, 51.80 Ma), indicating that the basal areas of muricae are not impervious to the deleterious effects of diagenesis.

[28] Measured muricae-$\delta^{18}O$ values from the late Paleocene, including the transient PETM warming pulse, are considerably lower than the Eocene values, and average −3.7‰ ($n = 68$). The lowest $\delta^{18}O$ values (−3.9‰ to −4.3‰) were measured in four tests of the PETM morphotype *M. allisonensis* (102.86–103.00 mbsf, Figures 5a and 5b), and in two tests of *M. velascoensis* (−4.4‰ and −4.5‰) from just above the PETM interval (102.4 and 102.7 mbsf).

4. Discussion

4.1. Preservation of Muricae

[29] The muricate genera *Morozovella* and *Acarinina* dominated planktonic foraminiferal faunas inhabiting the mixed layer of the tropical to subtropical ocean during the ~20 million years encompassing the time interval extending from the late Paleocene to the latest middle Eocene [*Wade*, 2004], and the evolutionary histories of these Early Paleogene muricate genera are well documented in the literature [e.g., *Blow*, 1979; *Kelly et al.*, 1996b; *Olsson et al.*, 1999; *Pearson et al.*, 2006]. Muricae typically occur at focal points for biogenic calcification situated at the intersections of interpore ridges, and are considered to be analogous to pustules seen on the tests of such modern planktonic foraminifera as *Globorotalia menardii* and *G. truncatulinoides* [*Blow*, 1979; *Olsson et al.*, 1999]. The adaptive functionality of muricae remains unclear, yet it is well established that muricae are primary, biogenic structures that developed

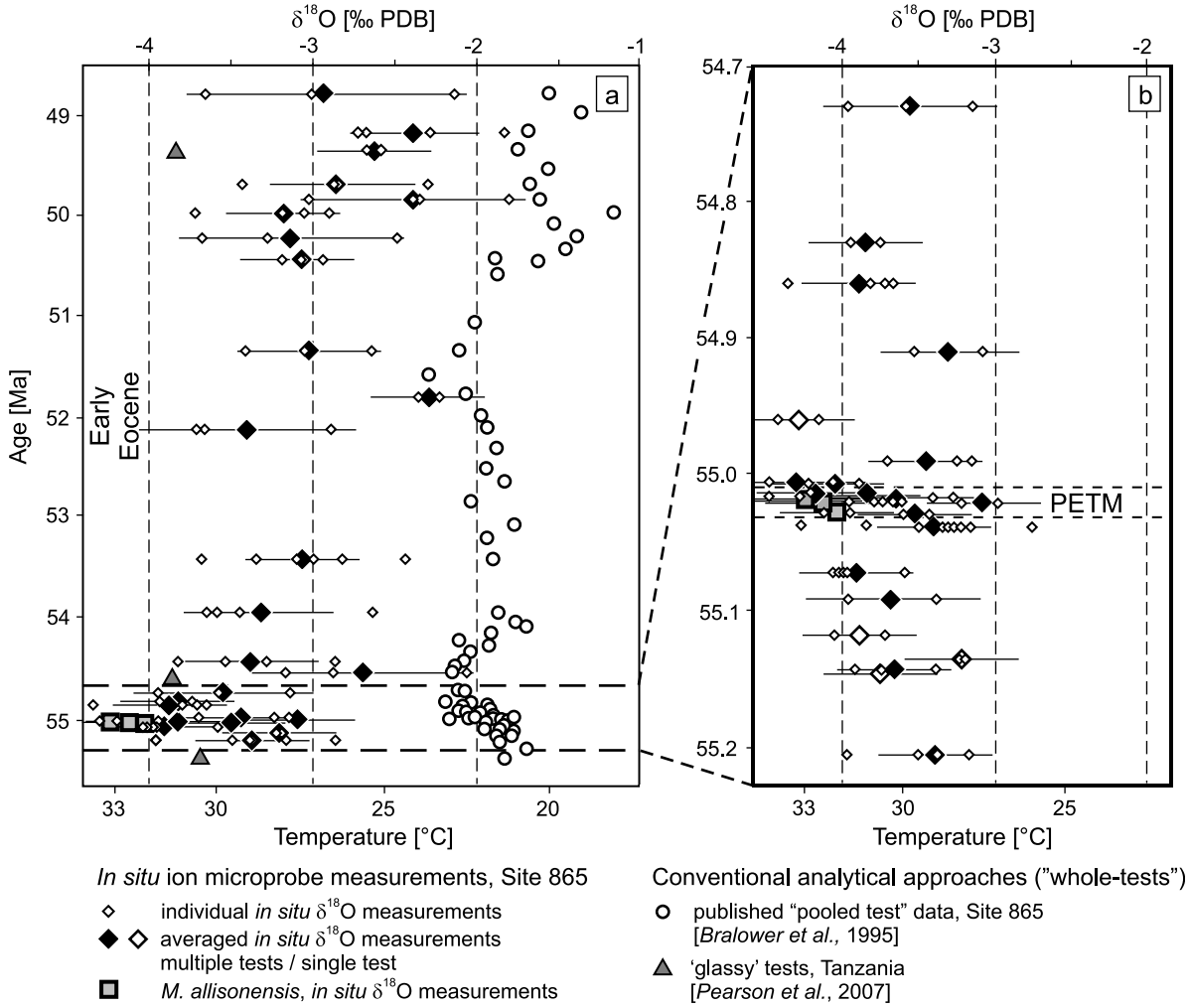

Figure 5. Parallel planktonic foraminiferal oxygen isotope and SST records for the late Paleocene to early Eocene interval of ODP Site 865, one measured in situ by ion microprobe at WiscSIMS and the other by conventional acid solution techniques. (a) Small white and large black diamonds are individual and averaged in situ muricae δ^{18}O values of morozovellids, respectively. Gray squares are averaged δ^{18}O of muricae bases from the PETM morphotype *M. allisonensis* (see text). Error bars represent ±2 standard error of the mean for multiple analyses. Previously published δ^{18}O values derived from acid solution analyses of pooled, multispecimen samples from the same core depth [*Bralower et al.*, 1995] are shown as open circles for comparison. In addition, δ^{18}O values of unaltered glassy morozovellids from Tanzanian drill cores [*Pearson et al.*, 2007] are plotted as gray triangles. In the densely sampled PETM interval, in situ δ^{18}O measurements are shown for every third core sample. (b) Enlargement of interval spanning the Paleocene-Eocene boundary showing complete PETM ion microprobe δ^{18}O data set.

during test calcification. However, this does not preclude the possibility that muricae in frosty planktonic tests have been subjected to some degree of postdepositional diagenesis. For instance, the granular, microcrystalline texture featured by muricae in unaltered glassy morozovellid tests is not readily recognized in the coarser, blade-like muricae of frosty morozovellids (Figure 6a) [*Sexton et al.*, 2006; *Pearson et al.*, 2007]. This observation led researchers to postulate that the coarser crystallites forming the prominent "blade-like towers" (Figure 6b) [*Sexton et al.*, 2006] on frosty morozovellids are the result of secondary, diagenetic calcification.

[30] In order to insure that in situ δ^{18}O analyses were performed on primary biogenic calcite, the shape and appearance of muricae on whole tests of glassy and frosty morozovellid specimens were evaluated by SEM and compared to dozens of high contrast backscattered electron images of morozovellid cross sections (see the auxiliary material). The muricae of unaltered, glassy morozovellid tests exhibit a microgranular structure that is characteristic of biogenic calcite (Figure 6a) [*Sexton et al.*, 2006]. This microgranular texture is retained at the base of most muricae in diagenetically altered frosty morozovellid tests (Figures 6b and 6c). As postulated by *Sexton et al.* [2006],

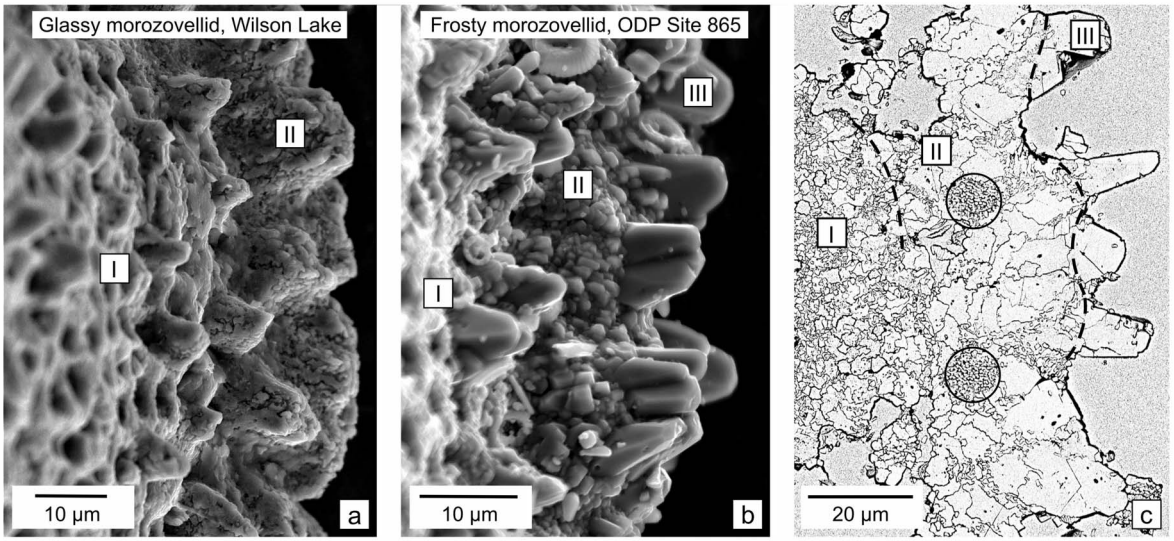

Figure 6. (a, b) SEM images of muricae on morozovellid tests. Figure 6a is a glassy morozovellid from the PETM section of Wilson Lake, New Jersey [*Zachos et al.*, 2006]. Figure 6b is a frosty morozovellid test from ODP Site 865 (Hole 865C, 103.10 mbsf). Point I indicates chamber walls, and point II indicates muricae. Their tips serve as focal points for diagenesis that results in enlarged blade-like "towers," the typical appearance of muricae on frosty planktonic foraminiferal tests (point III in Figures 6b and 6c) [*Sexton et al.*, 2006]. (c) Backscattered SEM image of the chamber wall and muricae of a frosty morozovellid test in cross section (ODP Site 865), highlighting different crystallinities. Point I indicates a fine-grained granular chamber wall; point II indicates medium-grained granular muricae. This "coarser" texture of the basal area of muricae does not conform to the strict definition for pristine biogenic calcite, so some degree of recrystallization may have occurred. Two ~10 μm diameter ion microprobe pits for δ^{18}O analysis are encircled. Textures in the pits are etched by the Cs^+ beam. Point III indicates rhombohedral diagenetic overgrowths. Accurate δ^{18}O measurements by ion microprobe cannot be obtained from the chamber wall (point I, Figure 6c) of frosty morozovellids due to microporosity and mural pores (compare to Figure 1d).

the tips of muricae serve as focal points for cementation that results in enlarged blade-like "towers" with distinct crystal faces, the typical appearance of muricae on frosty morozovellid tests (Figures 1a, 6b, and 6c). As a consequence, considerable effort was made to restrict in situ δ^{18}O analyses to the basal portion of the muricae where granular calcite is still present. Incidentally, we note that the coarser crystallites forming the tips of the muricae could not be targeted for in situ δ^{18}O measurements as their cross section is typically smaller than the diameter of the primary beam spot (~10 μm) required for high-precision, in situ analyses. However, some in situ measurements converge upon published whole test values, which may indicate that the analysis pit was placed in the transition between biogenic calcite and diagenetic crystallites.

[31] The resistance of the granular basal portion of muricae to postdepositional alteration may be explained by the absence of mural pores in these pustular outgrowths. Furthermore, muricae are formed from larger crystals than the remaining test (Figure 6). High contrast backscattered electron imaging indicates that the granular texture of the chamber wall is fine-grained with a high density of cross-cutting mural pores, whereas the granular texture at the basal domain of muricae is medium-grained (Figure 6c). We therefore attribute the diagenetically resistant, medium-grained texture of the basal domain of muricae to enhanced biocalcification that resulted from being located at the juncture of two prominent interpore ridges. In contrast, the extremities of the muricae on frosty morozovellids are elongated by coarse-grained, diagenetic crystallites that display rhombohedral cleavage in cross section.

[32] In this respect, it should be noted that pristine biogenic calcite is composed of irregular 'microgranules' (~0.1 μm) without clear crystal faces [e.g., *Bentov and Erez*, 2005]. In the process of recrystallization, these microgranules are replaced with larger, more equant crystals [*Pearson and Burgess*, 2008]. Thus, the 'coarser' texture of the basal area of muricae does not conform to the strict definition for pristine biogenic calcite, so some degree of recrystallization may have occurred. However, in a comparative textural study on high-latitude Eocene foraminifera, *Pearson and Burgess* [2008] concluded that even for some glassy samples, a small amount of recrystallization cannot be ruled out.

4.2. Mg/Ca in Muricae Calcite

[33] Precipitation experiments designed to calculate D_{Mg} for inorganic calcite [e.g., *Mucci and Morse*, 1983; *Mucci*, 1987; *Oomori et al.*, 1987] predict over an order of magnitude more Mg in inorganic calcite than in biogenic foraminiferal calcite [*Bentov and Erez*, 2006]. Therefore, the presence of even a small volume of diagenetic calcite is expected to elevate mean foraminiferal test Mg/Ca values, and greatly exceed those from well-preserved glassy foraminiferal samples. Figure 7 shows Mg/Ca ratio maps

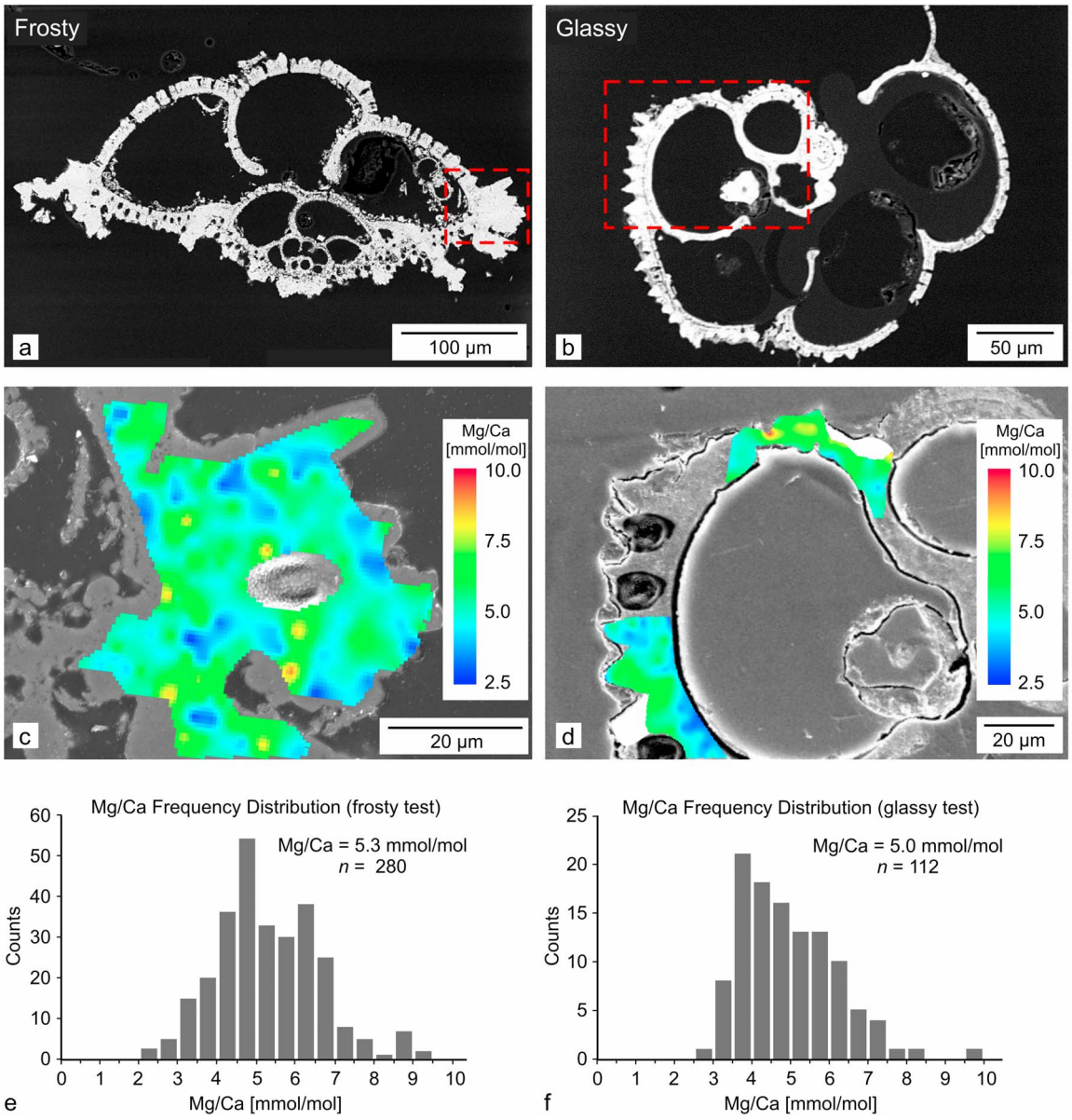

Figure 7. (a) Scanning electron microscope image of cross sections through a frosty test of *Morozovella velascoensis* (ODP Site 865, 103.1 mbsf) and (b) a glassy morozovellid test from the PETM section (108.37 m) recovered at Wilson Lake, New Jersey. (c, d) Mg/Ca composition ratio maps measured by electron probe micro analyzer (EPMA) of representative muricae outlined by the insets in Figures 6a and 6b. White areas in the Mg/Ca map of the glassy test were analyzed by EPMA, but elemental totals were below 96% as measurements were performed too close to the calcite/epoxy boundary which caused size or edge effects [*Fournelle*, 2006]. (e, f) The Mg/Ca ratios plotted as histograms. Averaged Mg/Ca ratios of representative muricae from frosty and glassy morozovellid tests are 5.3 and 5.0 mmol/mol, respectively, and comparable to published data from whole-test analyses [*Tripati et al.*, 2003; *Zachos et al.*, 2006].

measured by electron probe micro analyzer (EPMA) of representative muricae of a frosty morozovellid test from ODP Site 865 (same specimen as shown in Figure 1) and a glassy test from the Wilson Lake PETM section. Mg/Ca ratios of muricae from frosty and glassy morozovellid tests average 5.3 and 5.0 mmol/mol, respectively (X[Mg/Mg+Ca] ~0.005, Figure 7), and are comparable to published data from whole-test analyses of unaltered glassy tests [*Zachos et al.*, 2006].

[34] It is notable that significantly elevated Mg/Ca ratios were not detected in the blade-like crystallite protruding from the muricae of the frosty morozovellid test (Figure 7c). This finding contradicts the results of the aforementioned laboratory experiments. Two possible explanations might

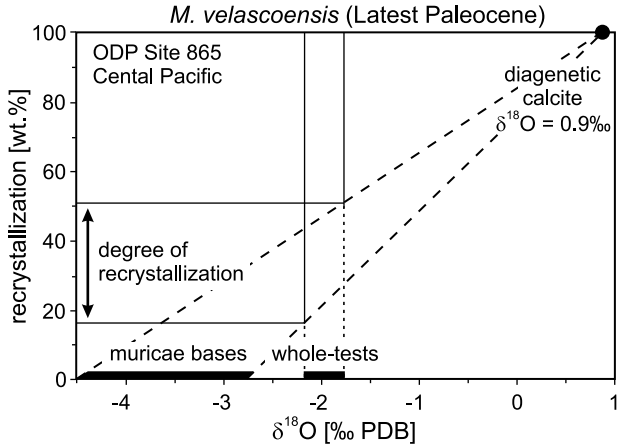

Figure 8. Model calculations of the effect of alteration on $\delta^{18}O$. The $\delta^{18}O$ in muricae bases on late Paleocene morozovellids from ODP Site 865 ranges from −2.8‰ to −4.5‰ (PDB; Table 2). Published whole test data of age equivalent samples from the same core [*Bralower et al.*, 1995] vary between −1.8‰ and −2.2‰. Assuming that the basal areas of muricae are unaltered and that diagenetic calcite has a $\delta^{18}O$ of 0.9‰ [*Schrag*, 1999; *Tripati et al.*, 2003], ~15–50 wt.% of the frosty morozovellid tests at Site 865 are recrystallized.

account for this inconsistency. First, it is possible that domains of high Mg/Ca were not detected by electron microprobe because the outer border of the analyzed area was several μm away from the outer surface of the morozovellid test. Alternatively, the D_{Mg} for inorganic calcite in deep-sea sedimentary sections is significantly lower than suggested by laboratory experiments. Previous studies performed on planktonic foraminiferal tests preserved in deep-sea sediments also found contradictory results. *Tripati et al.* [2003] and *Sexton et al.* [2006] report no evidence of significantly elevated Mg/Ca ratios from whole test analyses of frosty planktonics preserved in Early Paleogene deep-sea sediments recovered at low latitude sites. In contrast to these findings, *Regenberg et al.* [2007] measured Mg/Ca ratios of up to 40 mmol/mol in crystallites formed on foraminiferal tests from a tropical Atlantic deep-sea core, which closely matches Mg/Ca ratios predicted by inorganic precipitation experiments. Thus, the affect of diagenetic alteration on the Mg/Ca ratio of deep-sea carbonates is not fully understood and warrants further investigation in future studies.

4.3. Late Paleocene to Early Eocene Tropical SSTs Inferred From in Situ $\delta^{18}O$ Measurements

[35] Over the last decade, the reliability of planktonic $\delta^{18}O$ records used to estimate tropical SSTs for the Cretaceous and Paleogene greenhouse climate states has been called into question [e.g., *Pearson et al.*, 2001; *Norris et al.*, 2002; *Wilson et al.*, 2002; *Sexton et al.*, 2006]. The Cretaceous and Paleogene episodes of global warming are widely recognized as ancient analogs for current and future climate change, and are typified by exceptional polar warmth and deep-sea temperatures that were 8 to 12°C higher than today [*Zachos et al.*, 2003, 2008]. To the contrary, $\delta^{18}O$ records generated using frosty planktonic tests suggest that tropical SSTs peaked at only ~25°C during the Paleogene greenhouse climate (Figure 5) [*Bralower et al.*, 1995], which is below today's maximum of 27–30°C [*Ramanathan and Collins*, 1991] and substantially lower than SSTs (≥30°C) predicted by greenhouse gas–forced climate models [e.g., *Huber and Sloan*, 2000]. This data versus model mismatch in SSTs is referred to as the 'cool tropics paradox' [*D'Hondt and Arthur*, 1996]. Two explanations have been proposed to account for the cool tropics paradox, one envisions reduced latitudinal thermal gradients due to more efficient meridional oceanic heat transport to the poles [e.g., *Shackleton and Boersma*, 1981; *Barron*, 1987; *Rind and Chandler*, 1991; *Schmidt and Mysak*, 1996; *Lyle*, 1997; *Brady et al.*, 1998], while the other contends that the relatively cool $\delta^{18}O$-based SSTs are an artifact of postdepositional diagenesis that has biased planktonic $\delta^{18}O$ values toward more positive values [e.g., *Killingley*, 1983; *Schrag et al.*, 1992, 1995; *Wilson and Opdyke*, 1996; *Pearson et al.*, 2001; *Sexton et al.*, 2006].

[36] In situ $\delta^{18}O$ measurements by ion microprobe confirm that the cool tropics paradox is caused by postdepositional diagenesis of planktonic tests. The Site 865 muricae-$\delta^{18}O$ record indicates that SSTs in the tropical Pacific were substantially higher than those previously inferred from conventional $\delta^{18}O$ analysis of pooled, multispecimen samples [*Bralower et al.*, 1995]. Peak temperatures of 32–33°C are inferred from six $\delta^{18}O$ measurements performed on four tests of the short-lived PETM morphotype *M. allisonensis.* This PETM warming pulse is not clearly expressed in the published $\delta^{18}O$ record that is based on conventional whole-test measurements [*Bralower et al.*, 1995] (Figures 5a and 5b). Following this transient phase of PETM warming, the $\delta^{18}O$ in muricae bases of the planktonic species *M. subbotinae* and *M. aragonensis* indicate that SSTs cooled by 5°–7°C to ~27°C, and that early Eocene SSTs remained fairly constant over this period.

4.4. Assessing the Degree of Diagenetic Alteration at ODP Site 865

[37] If the $\delta^{18}O$ of basal areas of muricae represents the unaltered original value, then published $\delta^{18}O$ records of Site 865 include altered carbonate, and the climate events in the previously published record have been masked by diagenetic alteration of the planktonic tests. The degree of diagenetic alteration at ODP Site 865 can be assessed from mass balance (Figure 8). The two end-members selected for this calculation are (1) biogenic calcite forming the base of the muricae and (2) diagenetic calcite that is precipitated in the cold bottom water after foraminiferal deposition. Pore water measurements in cores from Site 865 show near-seawater $\delta^{18}O$ values [*Paull et al.*, 1995] and calcite formed during postdepositional alteration at this location are estimated to have $\delta^{18}O$ of ~0.9‰ PDB [*Tripati et al.*, 2003]. The $\delta^{18}O$ of late Paleocene muricae bases, including samples from the PETM interval, range from −2.8‰ to −4.5‰ (n = 69). Using these end-members, the difference in $\delta^{18}O$ of 0.6‰–2.7‰ between the basal areas of muricae and previously published whole-test values from the same core samples suggests that morozovellid tests at Site 865 contain ~15–50 wt.% secondary, diagenetic calcite (Figure 8). This degree of alteration closely matches models for diagenesis in deep-sea sediments that predict ~30 wt.% recrystallization

[*Schrag et al.*, 1995; *Schrag*, 1999; *Tripati et al.*, 2003]. Unfortunately, accurate in situ measurements of the δ^{18}O of chamber walls are not feasible due to the high density of mural pores, which has the undesired effect of low secondary ion yields and a nonreproducible shift in measured δ^{18}O.

4.5. Comparison of Muricae δ^{18}O-Inferred SSTs with Temperature Estimates From Glassy Foraminiferal Tests, TEX_{86} and Model Predictions

[38] Muricae δ^{18}O-based SST reconstructions for the late Paleocene to early Eocene greenhouse interval are in excellent agreement with published temperature estimates derived from unaltered glassy foraminiferal tests preserved in clay-rich sediments of hemipelagic deposits in Tanzania [*Pearson et al.*, 2001, 2007]. The lowest δ^{18}O value registered by the glassy tests from Tanzanian sediments straddling the Paleocene-Eocene boundary is −3.9‰ [*Pearson et al.*, 2007], corresponding to SSTs (31°–32°C) seldom reached in the modern ocean [*Huber and Sloan*, 2001]. However, δ^{18}O values published for early Eocene glassy planktonic tests are lower than δ^{18}O values in muricae bases of age equivalent samples from ODP Site 865 (Figure 5a). This discrepancy raises the possibility that some of domains targeted for in situ δ^{18}O analysis may be affected by diagenetic alteration.

[39] Muricae-δ^{18}O inferred SSTs are also supported by TEX_{86} measurements, a chemically independent proxy that is extracted from membrane lipids of marine crenarchaeota, which are a common component of picoplankton [*Schouten et al.*, 2003, 2004]. In a coupled TEX_{86}/isotope approach using core samples from Wilson Lake (New Jersey), *Zachos et al.* [2006] reported TEX_{86}-based SSTs for the PETM interval peaking at 33°C. These SSTs are identical to the muricae-δ^{18}O inferred SSTs derived from the short-lived PETM morphotype *M. allisonensis* at Site 865.

[40] In addition to the good agreement between muricae δ^{18}O-based SSTs and those inferred from glassy planktonic tests or chemically independent proxies such as TEX_{86}, the δ^{18}O of basal areas of muricae conform to model predictions. *Tindall et al.* [2010] used a General Circulation Model to estimate the δ^{18}O of past seawater, and thus to predict the δ^{18}O of planktonic tests under these conditions. For the present day, their model shows a good agreement between predicted and measured planktonic δ^{18}O; however, a significant mismatch exists between published 'whole-test' data from the Eocene low latitude ocean. The only data set matching predictions is the δ^{18}O record derived from glassy planktonics preserved in Eocene-aged deposits of Tanzania [*Pearson et al.*, 2001, 2007]. Model predicted foraminiferal δ^{18}O for Site 865 are approximately −3.5‰ [PDB] for the mixed layer (model simulation at 41.5–57.5 m water depth) and −4.0‰ for the surface ocean, which is in perfect agreement with the ion microprobe δ^{18}O measurements for Site 865.

4.6. Interspecific Differences in the Muricae δ^{18}O

[41] The short-lived (~170 ka) *Morozovella allisonensis* is one of three known morphotypes that are restricted to the PETM [*Kelly et al.*, 1996a]. The authors reported that *M. velascoensis* and *M. allisonensis* occupied distinctly different paleoecological niches. Using conventional whole-test measurements, *Kelly et al.* [1998] found consistently higher δ^{18}O values in *M. allisonensis*, suggesting that it inhabited a deeper depth habitat than *M. velascoensis*. Remarkably, this isotopic offset is reversed, as seen with the in situ δ^{18}O measurements by ion microprobe. The δ^{18}O of muricae bases in four tests of *M. allisonensis* within the Site 865 PETM interval vary from −4.3‰ to −3.9‰ and are 0.5‰–1‰ lower than average muricae δ^{18}O values of *M. velascoensis* from the same core samples (Figure 5b). We reconcile these conflicting findings by noting that the test of *M. allisonensis* is weakly calcified compared to that of *M. velascoensis*. Consequently, the 'whole-test δ^{18}O' of *M. allisonensis* is more sensitive to postdepositional alteration. Thus, in situ δ^{18}O measurements by ion microprobe indicate that the original, much lower δ^{18}O value is still preserved in the basal areas of muricae in *M. allisonensis*.

5. Conclusions

[42] This case study assesses the feasibility of ion microprobe technique for obtaining more reliable δ^{18}O values from moderately altered (frosty) tests of tropical planktonic foraminifera preserved in deep-sea sediments. To ground truth this novel approach, we performed in situ δ^{18}O measurements by ion microprobe on 10 μm diameter subdomains within individual tests of several planktonic species belonging to the mixed-layer dwelling genus *Morozovella* to generate a new tropical SST record for the Early Paleogene greenhouse climate state. Inspection of numerous tests by SEM and comparison to dozens of high contrast backscattered electron images of morozovellid cross sections revealed that the basal areas of muricae, pustular structures located at the intersections of interpore ridges on the test surfaces, retain the microgranular texture typifying biogenic calcite, while the blade-like crystallites accentuating the tips of muricae exhibit rhombohedral cleavage and are clearly diagenetic in origin. This interpretation was evaluated by employing EPMA to generate Mg/Ca ratio maps for the muricae on pristine, glassy and frosty, moderately altered morozovellid tests. Curiously, this high-resolution Mg/Ca ratio mapping technique did not detect elevated Mg levels within the muricae of frosty morozovellid tests as predicted by experimental studies; nevertheless, considerable effort was made to restrict all in situ δ^{18}O analyses to the basal areas of the muricae where granular calcite is still present to insure that these measurements were performed on biogenic calcite.

[43] In general, δ^{18}O values in the basal area of muricae are −0.6‰–−2.7‰ lower than published 'whole-test' δ^{18}O values generated via conventional acid dissolution techniques for age equivalent core samples from a late Paleocene to early Eocene (56–49 Ma) section recovered at ODP Site 865 in the central Pacific. Muricae δ^{18}O values for the late Paleocene average −3.7‰ with the lowest values (−3.9‰ to −4.3‰) measured from four tests of the PETM morphotype *M. allisonensis* and two tests of *M. velascoensis* (−4.4‰ and −4.5‰) from just above the PETM interval at Site 865. However, there are rare instances where in situ δ^{18}O measurements of early Eocene specimens temporarily converge upon published whole test values, suggesting that the basal areas of muricae are not completely impervious to the deleterious effects of diagenesis and/or the analysis pit over-

lapped with the transition between biogenic and diagenetic calcite.

[44] Assuming that the basal areas of muricae consist of biogenic calcite and retain their original $\delta^{18}O$ value, then the new ion microprobe $\delta^{18}O$ record indicates that tropical SSTs in the central Pacific were ~27°C during the early Eocene and reached at least ~33°C during the transient PETM warming pulse. Thus, SSTs inferred from the in situ $\delta^{18}O$ measurements are 4 to 8°C higher than those previously reported from conventional analytical approaches that entail whole-test digestion, and are generally consistent with climate model predictions, published SSTs derived from glassy foraminiferal tests, and TEX_{86} SST estimates.

[45] These results suggest that high-resolution backscatter electron imaging in combination with high analytical precision (±0.3‰, 2 SD) and high spatial resolution $\delta^{18}O$ analysis by ion microprobe can be used to enhance the fidelity of tropical SST records derived from moderately altered frosty foraminiferal tests, a state of preservation that is ubiquitous in the deep-sea sedimentary record. The findings of this investigation support the view that the 'cool tropics paradox' controversy surrounding the Cretaceous and Early Paleogene greenhouse climates may indeed be an artifact of postdepositional diagenetic alteration, which increased whole-test $\delta^{18}O$ values resulting in erroneously cool tropical SSTs. Although our findings clearly demonstrate the potential of ion microprobe analysis for extracting the wealth of paleoclimatic information encoded within foraminiferal tests from open-ocean settings, we caution that the Early Paleogene tropical SST record herein reported is still deemed provisional as it is predicated upon the interpretation that the basal areas of muricae represent unaltered subdomains within frosty planktonic foraminiferal tests. Further application of ion microprobe $\delta^{18}O$ analysis to generate tropical SST records awaits future testing and refinement.

[46] **Acknowledgments.** We are grateful to Brian Hess for the careful sample preparation. James Zachos kindly provided Wilson Lake samples. This study greatly benefited from fruitful discussions with Taka Ushikubo and technical support from Jim Kern. Reviews by Paul N. Pearson and Bridget S. Wade substantially improved this paper. We thank Rainer Zahn for editorial handling. This research was supported by DOE (93ER14389), NSF-EAR (0628719, 0838058), and the Wisconsin Alumni Research Association. The Ocean Drilling Program (ODP) supplied Site 865 samples. ODP is sponsored by the U.S. National Science Foundation (NSF) and participating countries under management of Joint Oceanographic Institutions (JOI), Inc. WiscSIMS is partly supported by NSF-EAR (0319230, 0744079, 1053466).

References

Barron, E. J. (1987), Eocene equator-to-pole surface ocean temperatures: A significant climate problem?, *Paleoceanography*, *2*, 729–739, doi:10.1029/PA002i006p00729.

Bé, A. W. H. (1968), Shell porosity of recent planktonic foraminifera as climate index, *Science*, *161*, 881–884, doi:10.1126/science.161.3844.881.

Bemis, B. E., H. J. Spero, J. Bijma, and D. W. Lea (1998), Reevaluation of the oxygen isotopic composition of planktonic foraminifera: Experimental results and revised paleotemperature equations, *Paleoceanography*, *13*, 150–160, doi:10.1029/98PA00070.

Bentov, S., and J. Erez (2005), Novel observations on biomineralization processes in foraminifera and implications for Mg/Ca ratio in the shell, *Geology*, *33*, 841–844, doi:10.1130/G21800.1.

Bentov, S., and J. Erez (2006), Impact of biomineralization processes on the Mg content of foraminiferal shells: A biological perspective, *Geochem. Geophys. Geosyst.*, *7*, Q01P08, doi:10.1029/2005GC001015.

Berggren, W. A., D. V. Kent, C. C. Swisher III, and M.-P. Aubry (1995), A Revised Cenozoic geochronology and chronostratigraphy, in *Geochronology, Time Scales and Global Correlation*, edited by W. A. Berggren et al., *Spec. Publ. SEPM Soc. Sediment. Geol.*, *54*, 129–212.

Blow, W. H. (1979), *The Cainozoic Globigerinida*, E. J. Brill, Leiden, Netherlands.

Bowman, J. R., J. W. Valley, and N. T. Kita (2009), Mechanisms of oxygen isotopic exchange and isotopic evolution of $^{18}O/^{16}O$-depleted periclase zone marbles in the Alta aureole, Utah: Insights from ion microprobe analysis of calcite, *Contrib. Mineral. Petrol.*, *157*, 77–93, doi:10.1007/s00410-008-0321-1.

Brady, E. C., R. M. DeConto, and S. L. Thompson (1998), Deep water formation and poleward ocean heat transport in the warm climate extreme of the Cretaceous (80 Ma), *Geophys. Res. Lett.*, *25*, 4205–4208, doi:10.1029/1998GL900072.

Bralower, T. J., and J. Mutterlose (1995), Calcareous nannofossil biostratigraphy of Site 865, Allison Guyot, central Pacific Ocean: A tropical Paleogene reference section, in *Northwest Pacific Atolls and Guyots: Sites 865–870*, *Proc. Ocean Drill. Program Sci. Results*, *143*, 31–74.

Bralower, T. J., J. C. Zachos, E. Thomas, M. Parrow, C. K. Paull, D. C. Kelly, I. P. Silva, W. V. Sliter, and K. C. Lohmann (1995), Late Paleocene to Eocene paleoceanography of the equatorial Pacific Ocean: Stable isotopes recorded at Ocean Drilling Program Site 865, Allison Guyot, *Paleoceanography*, *10*, 841–865, doi:10.1029/95PA01143.

Coplen, T. B., C. Kendall, and J. Hopple (1983), Comparison of stable isotope reference samples, *Nature*, *302*, 236–238, doi:10.1038/302236a0.

D'Hondt, S., and M. A. Arthur (1996), Late Cretaceous oceans and the cool tropic paradox, *Science*, *271*, 1838–1841, doi:10.1126/science.271.5257.1838.

D'Hondt, S., J. C. Zachos, and G. Schultz (1994), Stable isotopic signals and photosymbiosis in Late Paleocene planktic foraminifera, *Paleobiology*, *20*(3), 391–406.

Duplessy, J.-C., P. L. Blanc, and A. W. H. Bé (1981), Oxygen-18 enrichment in planktonic foraminifera due to gametogenic calcification below the euphotic zone, *Science*, *231*, 1247–1250.

Eiler, J. M., C. M. Graham, and J. W. Valley (1997), SIMS analysis of oxygen isotopes: Matrix effects in complex minerals and glasses, *Chem. Geol.*, *138*, 221–244, doi:10.1016/S0009-2541(97)00015-6.

Emiliani, C. (1955), Pleistocene temperatures, *J. Geol.*, *63*, 537–578, doi:10.1086/626295.

Emiliani, C. (1966), Isotopic paleotemperatures, *Science*, *154*, 851–857, doi:10.1126/science.154.3751.851.

Epstein, S., R. Buchsbaum, H. A. Lowenstam, and H. C. Urey (1951), Carbonate-water isotopic temperature scale, *Geol. Soc. Am. Bull.*, *62*, 417–426, doi:10.1130/0016-7606(1951)62[417:CITS]2.0.CO;2.

Epstein, S., R. Buchsbaum, H. A. Lowenstam, and H. C. Urey (1953), Revised carbonate-water isotopic temperature scale, *Geol. Soc. Am. Bull.*, *64*, 1315–1325, doi:10.1130/0016-7606(1953)64[1315:RCITS]2.0.CO;2.

Erez, J., and B. Luz (1983), Experimental paleotemperature equation for planktonic foraminifera, *Geochim. Cosmochim. Acta*, *47*, 1025–1031, doi:10.1016/0016-7037(83)90232-6.

Ferry, J. M., T. Ushikubo, N. T. Kita, and J. W. Valley (2010), Assessment of grain-scale homogeneity and equilibration of carbon and oxygen isotope compositions of minerals in carbonate-bearing metamorphic rocks by ion microprobe, *Geochim. Cosmochim. Acta*, *74*, 6517–6540, doi:10.1016/j.gca.2010.08.039.

Fournelle, J. H. (2006), Silicate peak shifts, spectrometer peaking issues and standard/specimen size discrepancies in EPMA: 3 bumps in the road to the goal of 1% accuracy, *EOS Trans. AGU*, *87*(52), Fall Meet. Suppl., Abstract MB51A-04.

Frerichs, W. E., M. E. Heiman, L. E. Borgman, and A. W. H. Bé (1972), Latitudinal variations in planktonic foraminiferal test porosity: Part 1. Optical studies, *J. Foraminiferal Res.*, *2*, 6–13, doi:10.2113/gsjfr.2.1.6.

Hemleben, C., M. Spindler, and O. R. Anderson (1989), *Modern Planktonic Foraminifera*, Springer, New York.

Huber, B. T., and L. C. Sloan (2000), Climatic responses to tropical sea surface temperature changes on a "greenhouse" Earth, *Paleoceanography*, *15*, 443–450, doi:10.1029/1999PA000455.

Huber, M., and L. C. Sloan (2001), Heat transport, deep waters and thermal gradients: Coupled simulation of on Eocene greenhouse climate, *Geophys. Res. Lett.*, *28*, 3481–3484, doi:10.1029/2001GL012943.

Kelly, D. C., T. J. Bralower, J. C. Zachos, I. P. Silva, and E. Thomas (1996a), Rapid diversification of planktonic foraminifera in the tropical Pacific (ODP Site 865) during the late Paleocene thermal maximum, *Geology*, *24*, 423–426, doi:10.1130/0091-7613(1996)024<0423:RDOPFI>2.3.CO;2.

Kelly, D. C., A. J. Arnold, and W. C. Parker (1996b), Paedomorphosis and the origin of the planktonic foraminiferal genus *Morozovella*, *Paleobiology*, *22*(2), 266–281.

Kelly, D. C., T. J. Bralower, and J. C. Zachos (1998), Evolutionary consequences of the latest Paleocene thermal maximum for tropical planktonic foraminifera, *Palaeogeogr. Palaeoclimatol. Palaeoecol.*, *141*, 139–161, doi:10.1016/S0031-0182(98)00017-0.

Killingley, J. S. (1983), Effects of diagenetic recrystallization on $^{18}O/^{16}O$ values of deep-sea sediments, *Nature*, *301*, 594–597, doi:10.1038/301594a0.

Kim, S.-T., and J. R. O'Neil (1997), Equilibrium and nonequilibrium oxygen isotope effects in synthetic carbonates, *Geochim. Cosmochim. Acta*, *61*, 3461–3475, doi:10.1016/S0016-7037(97)00169-5.

Kita, N. T., T. Ushikubo, B. Fu, and J. W. Valley (2009), High precision SIMS oxygen isotope analysis and the effect of sample topography, *Chem. Geol.*, *264*, 43–57, doi:10.1016/j.chemgeo.2009.02.012.

Kozdon, R., T. Ushikubo, N. T. Kita, M. Spicuzza, and J. W. Valley (2009), Intratest oxygen isotope variability in the planktonic foraminifer *N. pachyderma*: Real vs. apparent vital effects by ion microprobe, *Chem. Geol.*, *258*, 327–337, doi:10.1016/j.chemgeo.2008.10.032.

Lyle, M. (1997), Could early Cenozoic thermohaline circulation have warmed the poles?, *Paleoceanography*, *12*, 161–167, doi:10.1029/96PA03330.

McConnaughey, T. (1989), ^{13}C and ^{18}O isotopic disequilibrium in biological carbonates. II. In vitro simulation of kinetic isotope effects, *Geochim. Cosmochim. Acta*, *53*, 163–171, doi:10.1016/0016-7037(89)90283-4.

McCrea, J. M. (1950), On the isotope chemistry of carbonates and a paleotemperature scale, *J. Chem. Phys.*, *18*, 849–857, doi:10.1063/1.1747785.

Mucci, A. (1987), Influence of temperature on the composition of magnesian calcite overgrowth precipitated from seawater, *Geochim. Cosmochim. Acta*, *51*, 1977–1984, doi:10.1016/0016-7037(87)90186-4.

Mucci, A., and J. W. Morse (1983), The incorporation of Mg^{2+} and Sr^{2+} into calcite overgrowths: Influences of growth-rate and solution composition, *Geochim. Cosmochim. Acta*, *47*, 217–233, doi:10.1016/0016-7037(83)90135-7.

Norris, R. D. (1996), Symbiosis as an evolutionary innovation in the radiation of Paleocene planktic foraminifera, *Paleobiology*, *22*, 461–480.

Norris, R. D., K. L. Bice, E. A. Magno, and P. A. Wilson (2002), Jiggling the tropical thermostat in the Cretaceous hothouse, *Geology*, *30*, 299–302, doi:10.1130/0091-7613(2002)030<0299:JTTTIT>2.0.CO;2.

Olsson, R. K., W. A. Berggren, C. Hemleben, and B. T. Huber (1999), *Atlas of Paleocene Planktonic Foraminifera*, 252 pp., Smithsonian Inst. Press, Washington, D. C.

Oomori, T., H. Kaneshima, Y. Maezato, and Y. Kitano (1987), Distribution coefficient of Mg^{2+} ions between calcite and solution at 10–50°C, *Mar. Chem.*, *20*, 327–336, doi:10.1016/0304-4203(87)90066-1.

Orland, I. J., M. Bar-Matthews, N. T. Kita, A. Ayalon, A. Matthews, and J. W. Valley (2009), Climate deterioration in the Eastern Mediterranean as revealed by ion microprobe analysis of a speleothem that grew from 2.2 to 0.9 ka in the Soreq Cave, Israel, *Quat. Res.*, *71*, 27–35, doi:10.1016/j.yqres.2008.08.005.

Paull, C. K., P. D. Fullagar, T. J. Bralower, and U. Röhl (1995), Seawater ventilaton of Mid-Pacific guyots drilled during Leg 143, in *Northwest Pacific Atolls and Guyots: Sites 865–870*, *Proc. Ocean Drill. Program Sci. Results*, *143*, 231–241.

Pearson, P. N., and C. E. Burgess (2008), Foraminifer test preservation and diagenesis: Comparison of high latitude Eocene sites, in *Biogeochemical Controls on Palaeoceanographic Environmental Proxies*, edited by W. E. N. Austin and R. H. James, *Geol. Soc. Spec. Publ.*, *303*, 59–72.

Pearson, P. N., P. W. Ditchfield, J. Singano, K. G. Harcourt-Brown, C. J. Nicholas, R. K. Olsson, N. J. Shackleton, and M. Hall (2001), Warm tropical sea surface temperatures in the Late Cretaceous and Eocene epochs, *Nature*, *413*, 481–487, doi:10.1038/35097000.

Pearson, P. N., R. K. Olsson, C. Hemleben, B. T. Huber, and W. A. Berggren (Eds.) (2006), *Atlas of Eocene Planktonic Foraminifera*, *Spec. Publ. Cushman Found. Foraminiferal Res.*, vol. 41, 513 pp., Cushman Found., Fredericksburg, Va.

Pearson, P. N., B. E. van Dongen, C. J. Nicholas, R. D. Pancost, S. Schouten, J. M. Singano, and B. S. Wade (2007), Stable warm tropical climate through the Eocene Epoch, *Geology*, *35*, 211–214, doi:10.1130/G23175A.1.

Ramanathan, V., and C. B. Collins (1991), Thermodynamic regulation of ocean warming by cirrus clouds deduced from observations of the 1987 El Niño, *Nature*, *351*, 27–32, doi:10.1038/351027a0.

Regenberg, M., D. Nürnberg, J. Schönfeld, and G.-J. Reichart (2007), Early diagenetic overprint in Caribbean sediment cores and its effect on the geochemical composition of planktonic foraminifera, *Biogeosciences*, *4*, 957–973, doi:10.5194/bg-4-957-2007.

Rind, D., and M. Chandler (1991), Increased ocean heat transports and warmer climate, *J. Geophys. Res.*, *96*, 7437–7461, doi:10.1029/91JD00009.

Rohling, J. R., and S. Cooke (2003), Stable oxygen and carbon isotopes in foraminiferal carbonate shells, in *Modern Foraminifera*, edited by B. K. Sen Gupta, pp. 239–277, Kluwer Acad., New York.

Schiffelbein, P. (1986), The interpretation of stable isotopes in deep-sea sediments: An error analysis case study, *Mar. Geol.*, *70*, 313–320, doi:10.1016/0025-3227(86)90008-3.

Schiffelbein, P., and S. Hills (1984), Direct assessment of stable isotope variability in planktonic foraminifera populations, *Palaeogeogr. Palaeoclimatol. Palaeoecol.*, *48*, 197–213, doi:10.1016/0031-0182(84)90044-0.

Schmidt, G. A., and L. A. Mysak (1996), Can increased poleward oceanic heat flux explain the warm Cretaceous climate?, *Paleoceanography*, *11*, 579–593, doi:10.1029/96PA01851.

Schouten, S., E. C. Hopmans, A. Forster, Y. van Breugel, M. M. M. Kuypers, and J. S. S. Damste (2003), Extremely high sea-surface temperatures at low latitudes during the middle Cretaceous as revealed by archaeal membrane lipids, *Geology*, *31*, 1069–1072, doi:10.1130/G19876.1.

Schouten, S., E. C. Hopmans, and J. S. Sinninghe Damsté (2004), The effect of maturity and depositional redox conditions on archaeal tetraether lipid palaeothermometry, *Org. Geochem.*, *35*(5), 567–571, doi:10.1016/j.orggeochem.2004.01.012.

Schrag, D. P. (1999), Effects of diagenesis on the isotopic record of late paleogene tropical sea surface temperatures, *Chem. Geol.*, *161*(1–3), 215–224, doi:10.1016/S0009-2541(99)00088-1.

Schrag, D. P., D. J. DePaolo, and F. M. Richter (1992), Oxygen isotope exchange in a two-layer model of oceanic crust, *Earth Planet. Sci. Lett.*, *111*, 305–317, doi:10.1016/0012-821X(92)90186-Y.

Schrag, D. P., D. J. DePaolo, and F. M. Richter (1995), Reconstructing past sea surface temperatures: Correcting for diagenesis of bulk marine carbonate, *Geochim. Cosmochim. Acta*, *59*, 2265–2278, doi:10.1016/0016-7037(95)00105-9.

Sexton, P. F., P. A. Wilson, and P. N. Pearson (2006), Microstructural and geochemical perspectives on planktic foraminiferal preservation: "Glassy" versus "Frosty," *Geochem. Geophys. Geosyst.*, *7*, Q12P19, doi:10.1029/2006GC001291.

Shackleton, N. J., and A. Boersma (1981), The climate of the Eocene Ocean, *J. Geol. Soc.*, *138*, 153–157, doi:10.1144/gsjgs.138.2.0153.

Shipboard Scientific Party (1993), *Northwest Pacific Atolls and Guyots: Sites 865–870*, *Proc. Ocean Drill. Program Initial Rep.*, *143*.

Simstich, J., M. Sarnthein, and H. Erlenkeuser (2003), Paired $\delta^{18}O$ signals of *Neogloboquadrina pachyderma* (s) and *Turborotalita quinqueloba* show thermal stratification structure in Nordic Seas, *Mar. Micropaleontol.*, *48*, 107–125, doi:10.1016/S0377-8398(02)00165-2.

Spero, H., and D. W. Lea (1996), Experimental determination of stable isotope variability in *Globigerina bulloides*: Implications for paleoceanographic reconstructions, *Mar. Micropaleontol.*, *28*, 231–246, doi:10.1016/0377-8398(96)00003-5.

Thomas, D. J., J. C. Zachos, T. J. Bralower, E. Thomas, and S. Bohaty (2002), Warming the fuel for the fire: Evidence for the thermal dissociation of methane hydrate during the Paleocene-Eocene thermal maximum, *Geology*, *30*, 1067–1070, doi:10.1130/0091-7613(2002)030<1067:WTFFTF>2.0.CO;2.

Tindall, J., R. Flecker, P. Valdes, D. N. Schmidt, P. Markwick, and J. Harris (2010), Modelling the oxygen isotope distribution of ancient seawater using a coupled ocean-atmosphere GCM: Implications for reconstructing early Eocene climate, *Earth Planet. Sci. Lett.*, *292*, 265–273, doi:10.1016/j.epsl.2009.12.049.

Tripati, A. K., M. L. Delaney, J. C. Zachos, L. D. Anderson, D. C. Kelly, and H. Elderfield (2003), Tropical sea-surface temperature reconstruction for the early Paleogene using Mg/Ca ratios of planktonic foraminifera, *Paleoceanography*, *18*(4), 1101, doi:10.1029/2003PA000937.

Urey, H. C., H. A. Lowenstam, S. Epstein, and C. R. McKinney (1951), Measurements of paleotemperatures of the Upper Cretaceous of England, Denmark and the southeastern United States, *Geol. Soc. Am. Bull.*, *62*, 399–416, doi:10.1130/0016-7606(1951)62[399:MOPATO]2.0.CO;2.

Valley, J. W., and N. T. Kita (2009), *In situ* oxygen isotope geochemistry by ion microprobe, in *Secondary Ion Mass Spectrometry in the Earth Sciences*, *Short Course Ser.*, vol. 41, edited by M. Fayek, pp. 16–63, Mineral. Assoc. Can., Quebec, Quebec, Canada.

Valley, J. W., C. M. Graham, B. Harte, J. M. Eiler, and P. D. Kinny, (1998), Ion microprobe analysis of oxygen, carbon, and hydrogen isotope ratios, in *Applications of Microanalytical Techniques to Understanding Mineralizing Processes*, *SEG Rev. Econ. Geol.*, vol. 7, edited by M. A. McKibben, W. C. Shanks III, and W. I. Ridley, p. 73–97, Soc. of Econ. Geol., Littleton, Colo.

van Andel, T. H. (1975), Mesozoic/Cenozoic calcite compensation depth and the global distribution of calcareous sediments, *Earth Planet. Sci. Lett.*, *26*, 187–194, doi:10.1016/0012-821X(75)90086-2.

Wade, B. S. (2004), Planktonic foraminiferal biostratigraphy and mechanisms in the extinction of *Morozovella* in the late middle Eocene, *Mar. Micropaleontol.*, *51*, 23–38, doi:10.1016/j.marmicro.2003.09.001.

Waelbroeck, C., S. Mulitza, H. Spero, T. Dokken, T. Kiefer, and E. Cortijo (2005), A global compilation of late Holocene planktonic foraminiferal $\delta^{18}O$: Relationship between surface water temperature and $\delta^{18}O$, *Quat. Sci. Rev.*, *24*, 853–868, doi:10.1016/j.quascirev.2003.10.014.

Wilson, P. A., and B. N. Opdyke (1996), Equatorial sea surface temperatures for the Maastrichtian revealed through remarkable preservation of metastable carbonate, *Geology*, *24*, 555–558, doi:10.1130/0091-7613(1996)024<0555:ESSTFT>2.3.CO;2.

Wilson, P. A., R. D. Norris, and M. J. Cooper (2002), Testing the Cretaceous greenhouse hypothesis using glassy foraminiferal calcite from the core of the Turonian tropics on Demerara Rise, *Geology*, *30*, 607–610, doi:10.1130/0091-7613(2002)030<0607:TTCGHU>2.0.CO;2.

Wu, G., and W. H. Berger (1989), Planktonic foraminifera: Differential dissolution and the Quaternary stable isotope record in the west equatorial Pacific, *Paleoceanography*, *4*, 181–198, doi:10.1029/PA004i002p00181.

Zachos, J. C., M. W. Wera, S. Bohaty, M. L. Delaney, M. R. Petrizzo, A. Brill, T. J. Bralower, and I. Premoli-Silva (2003), A transient rise in tropical sea surface temperature during the Paleocene-Eocene Thermal Maximum, *Science*, *302*, 1551–1554, doi:10.1126/science.1090110.

Zachos, J. C., S. Schouten, S. Bohaty, T. Quattlebaum, A. Sluijs, H. Brinkhuis, S. J. Gibbs, and T. J. Bralower (2006), Extreme warming of mid-latitude coastal ocean during the Paleocene-Eocene Thermal Maximum: Inferences from TEX_{86} and isotope data, *Geology*, *34*, 737–740, doi:10.1130/G22522.1.

Zachos, J. C., G. R. Dickens, and R. E. Zeebe (2008), An early Cenozoic perspective on greenhouse warming and carbon-cycle dynamics, *Nature*, *451*, 279–283, doi:10.1038/nature06588.

J. H. Fournelle, D. C. Kelly, N. T. Kita, R. Kozdon, and J. W. Valley, Wisconsin Secondary Ion Mass Spectrometer Laboratory, Department of Geoscience, 1215 W. Dayton St., University of Wisconsin-Madison, Madison, WI 53706, USA. (rkozdon@geology.wisc.edu)